Marine Geology 441 (2021) 106596

Contents lists available at ScienceDirect

Marine Geology

journal homepage: www.elsevier.com/locate/margo

Bottom current-controlled Quaternary sedimentation at the foot of the Malta Escarpment (Ionian Basin, Mediterranean)

Michele Rebesco [a,*], Angelo Camerlenghi [a], Vanni Munari [a], Renzo Mosetti [a], Jonathan Ford [a,b], Aaron Micallef [c,d], Lorenzo Facchin [a]

[a] National Institute of Oceanography and Applied Geophysics – OGS, Italy
[b] Department of Geoscience and Mathematics, University of Trieste, Italy
[c] Marine Geology & Seafloor Surveying, Department of Geosciences, University of Malta, Malta
[d] Helmholtz Centre for Ocean Research, GEOMAR, Kiel, Germany

ARTICLE INFO

Editor: Adina Paytan

Keywords:
Sediment waves
Seismics
Bathymetry
Oceanography
Cyclicity
Mediterranean

ABSTRACT

A better understanding of the evolution of bottom current circulation and associated deposits is significant for many applications including paleoclimatology and geological hazard. Besides the large contourite drifts, bottom currents may generate fields of large sediment waves that, depending on their height and velocity of migration, may pose severe risk for infrastructures. Conversely, the time span of their paleoceanographic record is generally relatively short. We use bathymetry data, sub-bottom and seismic reflection profiles and legacy oceanographic data to analyze the sediment waves occurring in a deep environment (from 2400 to 3800 m water depth at the foot of the Malta Escarpment in the Mediterranean Sea) to understand their evolution in time, their significance for paleoceanography, and their relation to present day hydrographic conditions. In the absence of direct stratigraphic information, we use the information from nearby studies and from ODP Site 964 and DSDP Site 374 to constrain the age of the sedimentary successions. We discover that these waves (about 2.5 km in wavelength, 50 m in height, with crest sub-perpendicular to the continental slope trend) have been steadily growing and migrating northward since about 500 ka, although an irregular growth and unsteady migration is distinguishable since about 1800 ka. The waves are generated by predominantly alongslope southward flowing bottom currents compatible with modern hydraulic conditions (mean flow speed of ~5 cm s^{-1}, peaks of 15 cm s^{-1}). The rate of crest migration (~ 2.0–3.2 mm a^{-1}) and the average sedimentation rate (0.64–0.69 mm a^{-1}) are unusually high for deep sea environments away from turbidity currents paths. We infer that the steady development of sediment waves is produced by a drastic increase in sediment input to the Ionian Basin resulting from the tectonic uplift in NE Sicily and Calabria and the onset of a relatively steady, low energy bottom current regime following the Mid-Pleistocene Transition. We attempt to extract information on orbital cyclicity preserved in the seismic record from the power spectra of virtual seismic traces from the well preserved succession of 5 visually discernible, regularly spaced sub-units consisting of alternation of high-amplitude and low-reflectivity packages within the last 500 ka. Peaks in the power spectra can be identified around orbital obliquity and precession periodicities, while eccentricity appears not to be recorded. We discuss the results of seismic cyclicity analysis relative to uncertainties of stratigraphic and petrophysical constraints. The sediment waves along the foot of the Malta escarpment are an excellent candidate for the extraction of a long, continuous and high resolution sedimentary record of the paleo circulation changes and climate cycles in the Mediterranean Sea since about 500 ka.

1. Introduction

The influence of bottom-water circulation in deep-sea sedimentation is still poorly understood, but the perception of its widespread importance is steadily increasing (Rebesco et al., 2014; Hernández-Molina et al., 2016; Mosher et al., 2017). New findings of contourites - sediments deposited or substantially reworked by the persistent action of bottom currents (Heezen et al., 1966; Stow et al., 2002a) - have been reported in many different settings in every ocean basin and even in lakes (Ceramicola et al., 2002; Van Daele et al., 2016). Contourite

* Corresponding author.
E-mail address: mrebesco@inogs.it (M. Rebesco).

https://doi.org/10.1016/j.margeo.2021.106596
Received 6 February 2021; Received in revised form 2 August 2021; Accepted 3 August 2021
Available online 12 August 2021

research is crucial for hydrocarbon exploration, paleoclimatology and paleoceanography. In fact, the persistent action of bottom currents may create large sedimentary bodies (contourite drifts) that provide valuable insights into paleoenvironmental and paleoclimatic conditions (Grützner et al., 2003; Villa et al., 2003; Lucchi and Rebesco, 2007; Hillenbrand et al., 2008). Bottom currents, predominantly unidirectional water currents that are in contact with the sea-floor or a sidewall (Zenk, 2008), are in fact pervasive and observed at all latitudes. Such currents, affected by tides, eddies, deep-sea storms, internal waves and tsunamis, are focused against continental slopes, escarpments and around topographic obstacles (see in-situ observations in Giorgetti et al., 2003; Zhao et al., 2015, Miramontes et al., 2019; Tallobre et al., 2016; Zhang et al., 2016).

Alongslope bottom currents flowing across the seabed are capable of actively eroding, transporting and depositing sediments on the seafloor, generating bedforms and relief, including sediment waves (Hernández-Molina et al., 2018). In early studies of the 1960s, which relied to a large extent on sub-bottom and seismic profiles, sediment waves were generally assumed to indicate the presence of bottom currents (Heezen, 1959), but in the 1970s it was recognized that sediment waves may be related to either bottom and turbidity currents (Embley and Langseth, 1977; Damuth, 1979). Subsequently, it was recognized that bottom current waves reflect a long-term response to environmental conditions (Flood and Shor, 1988) and the model for the generation of sediment waves beneath steady, sediment-laden bottom currents was put forward (Flood, 1988; Blumsack and Weatherly, 1989). It was also recognized that bottom current direction and velocity, both in present-day and in the past, may be estimated from sediment waves characteristics (Kenyon, 1986; McCave and Carter, 1997). Global reviews of seafloor bedforms were conducted by Wynn and Stow (2002) and Symons et al. (2016). Since then, many studies on sediment waves focused on the implications for the migration history of bottom water flows, but also on the associated geo-hazard (Putans et al., 2010; Bastia et al., 2011; Martin et al., 2015; Chen et al., 2017; Li et al., 2020). In fact, bottom currents are significant for slope-stability and assessment of geological hazards. The currents may pose a risk to deep-sea infrastructure such as pipelines and telecommunication cables, subsea oil and gas installations, moorings, or multidisciplinary observatories like the KM3NeT-It Cherenkov neutrino telescope (Margiotta, 2016), which is being constructed offshore the Malta Escarpment in the central Mediterranean Sea.

In the 1990s, large-scale asymmetric, climbing bedforms interpreted as sediment waves were identified at the foot of the Malta Escarpment (Marani et al., 1993). They were later imaged by Gutscher et al. (2016) and San Pedro et al. (2017) and regarded as being consistent with downslope turbidite transport. We now describe these sediment waves on the basis of recently acquired multi-channel seismic, sub-bottom

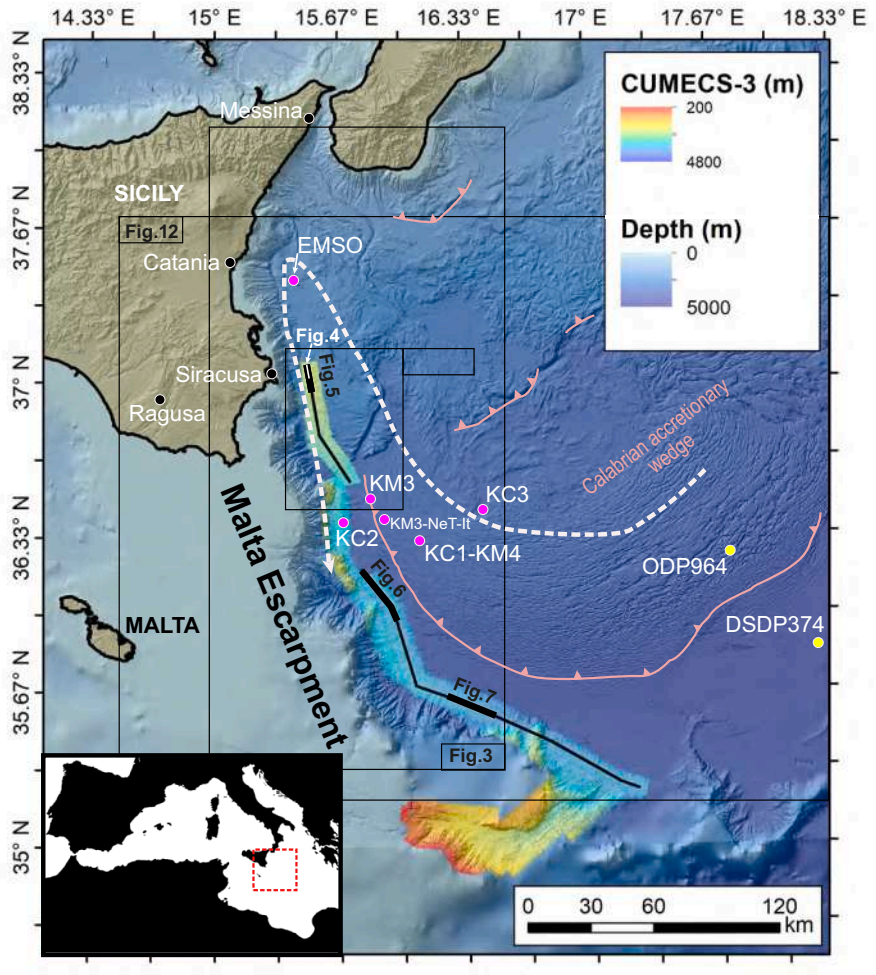

Fig. 1. Location map. Bathymetry base from a compilation of datasets including the compilation published by Gutscher et al. (2017) and CUMECS-3 data. Positions of Fig. 3 and S1 (sediment wave field), sub-bottom (Fig. 4) and seismic profiles (Figs. 5–7), Fig. 12 (average current field), of moorings (see Table 1) and of KM3NeT-It, of DSDP Site 374 and ODP Site 964 are shown.

echosounder and multibeam bathymetry data, and discuss their origin by considering available hydrographic information. The general aim of this study is to improve our understanding of sediment wave evolution in a deep sea environment. The specific aims are twofold: (i) to understand whether these features are still actively migrating and if they are a potential hazard for infrastructures; and (ii) to decipher their origin and their paleoceanographic significance.

2. Regional setting

2.1. Geological background

The study area is located within the Ionian Sea, at the foot of the Malta Escarpment between about 37°N and 35°N latitude (Fig. 1). In particular, we focus on a southward deepening deep-sea passageway at 2400 to 3800 m water depth between the Malta Escarpment and the Calabrian Accretionary Wedge.

The Malta Escarpment is a steep carbonate cliff about 300 km long and 3 km high that extends from offshore SE Sicily southwards and that locally reaches slope gradients of several tens of degrees (Micallef et al., 2016, 2019). The escarpment originated through a process of Tethyan continental rifting from Permian to Early Cretaceous, followed by lithospheric spreading in the Ionian basin. The passive margin transformed into an active tear fault with an additional sinistral strike-slip component in response to plate subduction of the Calabrian Arc system (e.g. Gutscher et al., 2016; Finetti, 1982; Nicolich et al., 2000; Polonia et al., 2016).

The Calabrian Accretionary Wedge is part of the Apennine accretionary system and consists of SE-verging thrust sheets composed of deformed Mesozoic and Cenozoic sediments scraped from the subducting Ionian oceanic lithosphere (Rossi and Sartori, 1981; Cernobori et al., 1996; Volpi et al., 2017). The seafloor of the western Ionian Basin is intensely affected by tectonic deformation, amplified by Messinian salt deformation in the shallow subsurface (Camerlenghi et al., 2020), which has resulted in a complex seafloor morphology to the east of the Malta Escarpment (Gutscher et al., 2017).

The presence of contourites east of the Malta Escarpment (in the form of large sediment waves, sediment drifts and associated moats) has been associated with the flow of bottom currents of Modified Atlantic Water, Levantine Intermediate Water and Adriatic Deep Water (Marani et al., 1993; Micallef et al., 2016; Pepe et al., 2018). The whole Plio-Quaternary sedimentary succession in the western Ionian Basin is interpreted to consist of fine-grained pelagics, contourites and turbidites with the shallower succession locally shaped into sediment waves (Micallef et al., 2018). On the basis of single-channel sparker seismic reflection profiles, large-scale asymmetric, climbing sediment waves were identified at the foot of the Malta Escarpment (Marani et al., 1993). These were tentatively ascribed to the action of bottom current intensification due to boundary current focussing along the very steep Malta Escarpment. More recently, the corridor between the north-western extremity of the Calabrian Accretionary Wedge and the Malta escarpment has been interpreted based on bathymetric data as a “turbidite valley” being formed by canyons and channels shaped by turbidity currents and the sediment waves therein as being consistent with downslope turbidite transport (Gutscher et al., 2016; San Pedro et al., 2017).

2.2. Hydrographic setting

The circulation patterns in the area are relatively well known only in the upper surface layer. In the upper hundreds meter depth, the Atlantic water flows eastward through the Sicily Channel and the northern branch (Atlantic Ionian Stream, Robinson et al., 1999) after the Malta escarpment is a broad open ocean free jet located approximately around 36—35°30’ N (Pinardi et al., 2015). The main water mass flowing along the western Mediterranean continental slope is the Levantine Intermediate Water (LIW; Wüst, 1961), which is by far the largest water mass produced in the Mediterranean Sea (Skliris, 2014).

The Adriatic Deep Water, formed mainly by the mixing of the surface water in the center of the South Adriatic Pit during periods of deep convection and exported to the Ionian in the bottom layer of the Strait of Otranto, represents the most important component of the bottom water of the entire Eastern Mediterranean (Gačić et al., 2001).

The upper Ionian Sea is a region where water masses of the main thermohaline circulation cell of the central and eastern Mediterranean converge. Permanent and seasonal eddies are present. The Ionian Basin, floored by a 4000 m deep abyssal plain, is filled by dense water from Adriatic and Aegean sources. Conductivity, temperature and depth (CTD) casts conducted between the years 2003 and 2010 as part of an international investigation program of the Eastern Mediterranean (Sparnocchia et al., 2011) are the only existing data that constrain abyssal water mass circulation in this area.

The distribution of dissolved oxygen concentration (DO), temperature, salinity and density in the central Ionian Sea demonstrates a strong interaction between the Adriatic outflow and waters of Aegean origin positioned above them, especially in the northern Ionian Sea (Bensi et al., 2013).

The Ionian abyssal circulation plays an important role in the redistribution of water masses to adjacent seas. Dense water masses formed by convection are often spread through the abyss by bottom-arrested currents (Hainbucher et al., 2006), which represent a significant mechanism for mixing in deep layers (Jungclaus and Backhaus, 1994). Because mesoscale eddies are often very efficient in transferring particles and passive tracers vertically or horizontally, both mean and mesoscale flows can contribute to the propagation and mixing of water masses in the Ionian Sea.

In the framework of the KM3NeT-It project (Margiotta, 2016), an intense programme of oceanographic observations was conducted in the Ionian Sea, mainly south-east of Capo Passero (Sicily), one of the three candidate sites to host the abyssal neutrino telescope. The activity included six hydrographic cruises and continuous bottom current hourly records from moorings in about 3100 m water depth from May 2007 until May 2009 at site KC1, and until March 2008 at two sites, KC2 and KC3 (Fig. 2). In general, current intensity is variable, even though the direction is relatively constant (Sparnocchia et al., 2011). In Sites KC1 and KC3, located far to the east with respect to the Malta Escarpment, the predominant direction of bottom water flow is northward. At Site KC2, located at the foot of the Malta Escarpment and closest to the sediment waves under investigation, the predominant direction is constantly to the SSW (Fig. 2). Measured bottom current flow directions in the area are also available at the EMSO-SN1 and KM3 sites (respectively LoBue, 2019 and Manca et al., 2002, 2003). Table 1 provides a summary of the bottom current flow direction at all available sites.

Rubino et al. (2012) attributed the variability of abyssal currents in the Ionian sea to mesoscale vortices (order of 10 km in the horizontal dimension) generated by baroclinic instability.

3. Data and methods

The study is based on geophysical data collected during the CUMECS-3 cruise, performed on board the R/V OGS Explora in March 2015 as part of a joint collaboration between OGS and the University of Malta.

3.1. Multibeam echosounder

Hull-mounted Reson Seabat 7150 (12/24 kHz) and a Reson Seabat 8111 (~100 kHz) echosounders were used during the cruise. The bathymetric data were acquired using PDS2000 software whereas editing and processing were carried out with MB-System software. The final bathymetry grid has a cell size of 60 m. The new bathymetric data covers the area along the foot of the Malta Escarpment and into the

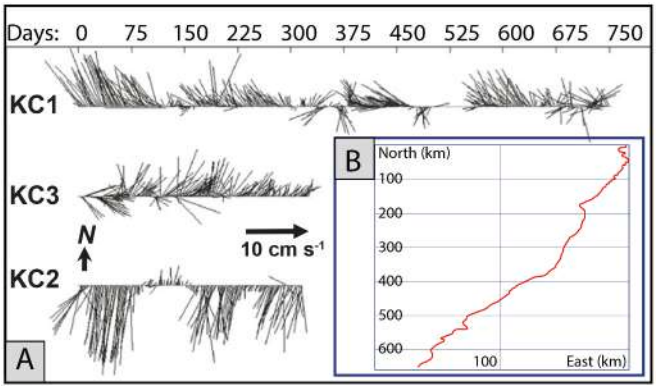

Fig. 2. Current data collected in the frame of KM3NeT-It project. A) Current stick plots at the three sites in the study area (from Sparnocchia et al., 2011). For a simplified visual representation, original hourly data are passed with a low-pass filter (48 h cutoff period) and resampled every 24 h. For the location of the mooring sites see also Fig. 1) Progressive vector diagram of the bottom current measured at KC2 site from 09/05/2007 to 11/03/2008 showing a direction towards SSW of the current. X-axis is representing the East coordinate (km) and y-axis the North coordinate (km). The average speed (computed from the data) is of the order of 5 cm s^{-1} with persistent peaks of 15 cm s^{-1}). From Schroeder and Borghini, 2008.

Heron Canyon, a total of 3400 km^2 (Fig. 1).

We also used other bathymetric datasets for the maps in this paper. These include the compilation published by Gutscher et al. (2017) using data from the following projects (cell size in parentheses): CIRCEE (60 m), M111 DIONYSUS (60 m), M112 (60 m), M86-2 (30 m), SHOM (60 m), CHIANTI (60 m), EMODNET (250 m), SRTM (75 m).

3.2. Sub-bottom profiler

A hull-mounted sub-bottom profiler Benthos CHIRP II was used during the CUMECS-3 survey simultaneously with the multibeam and reflection seismic acquisition. This instrument has a non-impulsive high frequency source that generates a continuous frequency sweep from 2 to 7 kHz. The transducer, model AT471, is composed of 16 elements that emit the sweep, with a maximum ping rate of 12 pings per second. Data were processed using the SwanPro and ChirpScanII software for application of automatic gain control (AGC) and cross-correlation.

3.3. Reflection seismics

The survey consisted of a short-offset, high-resolution multichannel seismic reflection data acquisition set up that was used along one composite profile following the flat seafloor at the foot of the Malta Escarpment. The composite profile comprises profiles CUMECS15-01, 02, 03 with a total length of 260 km (Fig. 1). The acquisition parameters are described in Table 2. Data processing was carried out at OGS using "Vista Seismic Processing 7.0" software. The processing flow involved band-pass filter 12/24–250/500 Hz, trace editing, geometric spreading correction, re-sampling (to 1 ms), velocity analysis and stacking, post-stack spiking deconvolution, post-stack time migration with finite difference method, and time-variant filtering. Although the velocity analysis was performed in order to stack the common midd-point traces, the short streamer length compared to the depth of the target is insufficient to derive meaningful interval velocities to be used to locate key-reflectors in depth and calculate thickness of seismic units. All illustrations in this paper show the final processed post-stack time-migrated sections. All data have been interpreted with (IHS) Kingdom 8.8 software.

3.4. Data interpretation

The nomenclature of Messinian Salinity Crisis (MSC) seismic markers follows Lofi et al. (2011). Data interpretation of the MSC seismic units, the Zanclean megaflood mass-transport deposit (MTD) and the overlying Plio-Quaternary cover follows the scheme published by Camerlenghi et al. (2020), Micallef et al. (2018, 2019) Spatola et al. (2020), and Garcia-Castellanos et al. (2020). Here the MTD was produced by the instantaneous invasion of Atlantic sea water that, after filling the western Mediterranean, spilled over the Sicily Sill to fill the eastern Mediterranean basin at the end of the Messinian Salinity Crisis.

Litho- and chrono-stratigraphic correlation of the seismic reflection data makes use of the closest scientific drilling boreholes (at about 150 km from our study area), namely Deep Sea Drilling Project (DSDP) Leg 42A, Site 374, located in 4088 m water depth in the Ionian Abyssal Plain (Shipboard Scientific Party, 1978), and Ocean Drilling Program (ODP) Leg 160 Site 964 located in 3662 m water depth on the outer reaches of the Calabrian Accretionary Wedge bordering the Ionian Abyssal Plain (Shipboard Scientific Party, 1996).

Megaturbidites below the Ionian Abyssal Plain, used for seismic and lithologic data correlation, were described by Hieke (2000): the ~650 ka old, up to 35 m-thick "Thick Transparent Layer - TTL"; the ~230 ka old, up to 7 m-thick "Deeper Transparent Layer – DTL"; and the CE 365 up to 20–25 m-thick AT (Augias Turbidite, dated by Polonia et al.,

Table 2
Acquisition parameters of CUMECS-3 multichannel seismic reflection data.

Vessel	OGS EXPLORA
Recording date	March 2015
Recorder	Geometrics GeoEel Digital
Data length	7 s
Sample rate	0.5 ms
Field filters	Low Cut 3 Hz
Coverage	8–10 fold
Navsystem	GPS - XSEA Octans interfaced with PDS2000
Energy source	Pneumatic source GI-Guns
Source array	1× cu.in GI-Gun in Harmonic Mode and 1× Mini GI-Gun in Harmonic Mode. Total volume 270 cu.in (4.4 l)
Depth of source	1.5 m ± 0.5 m
Streamer length	300 m
Number of traces	96
Group interval	3.125 m
Shot interval	15.625 m and 18.75 m
Depth of streamer	1.5 m ± 0.5 m
Near offset	18 m
Far offset	318 m

Table 1
Synthesis of available current meter data (see text for data references).

Station	Lat N	Lon E	Max current	Mean current	Mean direction (from N)	Direction
			cm s^{-1}	cm s^{-1}		
KC1	36°18′58.00″	16°05′33.00″	12	5	337.5	NNW
KC2	36°23′58.00″	15°40′60.00″	15	5	190.0	SSW
KC3	36°26′57.64″	16°25′59.46″	10	5	22.5	NNE
KM3	36°30′00.00″	15°49′60.00″	10	5	0.0	N
EMSO (SN1)	37°26′31.98″	15°25′35.22″	13	3.5	337.5	NNW

2013).

3.5. Seismic cyclostratigraphy

The approach to extract sediment cyclicity from the power spectrum of seismic traces follows that of Horn and Uenzelmann-Neben (2016), adapted for the dipping stratal geometry of the sediment waves. Virtual seismic traces are extracted on the stoss flank of the sediment waves, in the direction of increasing age, i.e., roughly perpendicular to the bedding reflections. The traces are trimmed to include only the target interval, i.e. the sediment wave-dominated succession from the seabed reflection to the onset of sediment wave deposition. The Two-Way Travel Time (TWTT) is converted to geological age by assuming the age in ka of the bounding reflections. A Hamming taper (with a half-width of 50 samples) is applied to the beginning and end of the traces to prevent high amplitudes from the bounding reflections from contaminating the power spectrum. The age-domain power spectrum of the virtual traces is estimated from the squared absolute Fast Fourier Transform (FFT) of the virtual traces.

Because we have no reliable information on the seismic velocities within the selected interval, and because we assume a constant rate of deposition, the intermediate step of converting the traces from TWTT to depth domain before converting to age domain is unnecessary (as in Horn and Uenzelmann-Neben, 2016).

4. Results

4.1. Seabed morphology

The CUMECS-3 bathymetric swath shows a wide field of undulations characterising sediment waves on the seafloor at the foot of the Malta Escarpment in water depths between ~2450 m and ~ 3800 m (Fig. 3). The seafloor undulations are elongated in a roughly NE-SW direction, approximately perpendicular to the trend of the Malta Escarpment. They are characterized by variable heights, from ~30 m to ~50 m (Fig. 4), with maximum height in the northern part, while their wavelength is around 2500 m. The wave crests are clearly marked by sinuosity and bifurcations (Fig. S1).

The compilation of existing bathymetric data reveals that similar undulations are present in an extensive area (Fig. 3), located preferentially in bathymetric lows that mark the transition between the steep continental slope of Sicily and the Malta Escarpment, to the west, and the gentle topography created by incipient sediment deformation of the outer Calabrian Arc, to the east.

4.2. Shallow subsurface structure

The sub-bottom profiler data reveal that the geometry of the seafloor defining the sediment waves is also replicated, in two dimensions, in the shallow subsurface (~ 50–70 m below the seafloor) by seismic reflections with wavy geometry that maintain the surface asymmetry of the sediment waves (Fig. 4). Sediment wave crests have clearly migrated towards the NNW through time. The seismic reflections are more widely spaced on the NNW flank, representing a thicker sedimentary succession, and closely spaced on the SSE flank, outlining thinner successions or even erosion. The dimensions of crests and troughs are generally comparable (about 2.5 km), with troughs not markedly narrower than the crests.

4.3. Deep sub-surface structure

4.3.1. Messinian Salinity Crisis units

The most obvious Messinian Salinity Crisis (MSC) marker is the Mobile Unit (MU - 3b) composed of halite and characterized by apparently transparent seismic facies that typically display ductile deformation. MU represents the seismic basement in our seismic reflection data

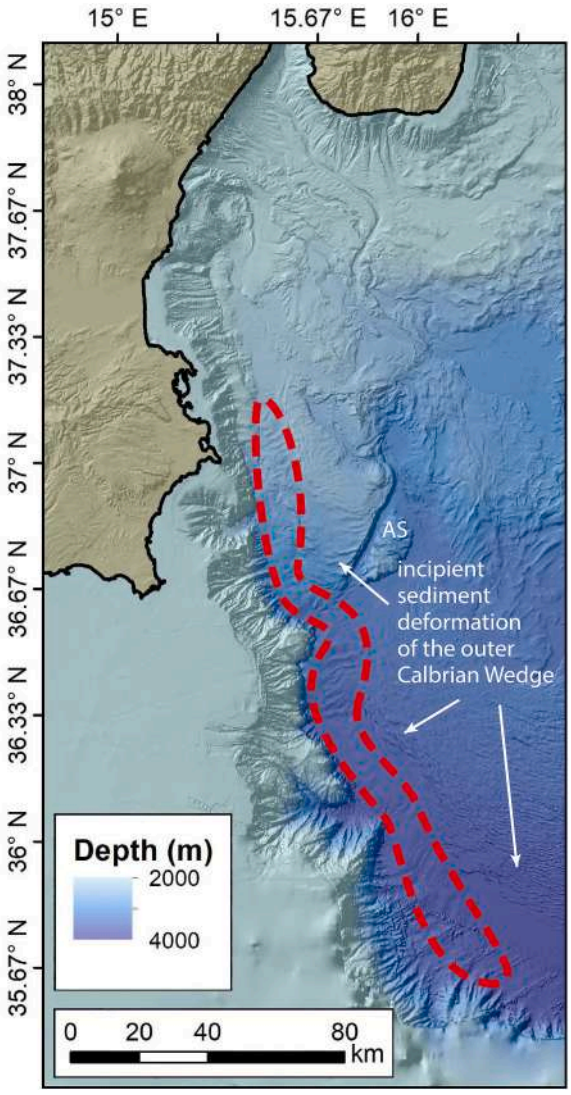

Fig. 3. Location of the field of sediment waves (outlined by the dashed red line) in the bathymetric low ("turbidite valley" of Gutscher et al., 2016; San Pedro et al., 2017) between the Malta Escarpment/Eastern Sicily margin and the gentle topography created by incipient sediment deformation of the outer Calabrian Accretionary Wedge superposed onto the regional shaded-relief multibeam bathymetry (from Gutscher et al., 2017 in addition to that of the CUMECS3 project). AS: Alfeo Seamount. Location of the area displayed in Fig. 1. (For interpretation of the references to colour in this figure legend, the reader is referred to the web version of this article.)

(Figs. 5–7).

MU is overlain by a high-amplitude reflective Upper Unit (UU - 3a) mainly composed of gypsum and anhydrite, with intercalated marls and dolomites. UU is well expressed in the southernmost part of the survey (Figs. 6, 7). Northwards, instead, UU is not detected either because it is absent, or because it was eroded during the deposition of the overlying unit.

Above UU or MU (when UU is absent) is a thick complex (Unit 2) with predominantly apparently chaotic internal configuration. In Fig. 6 Unit 2 thins gradually towards the SSE and its internal configuration changes laterally and vertically from apparently chaotic to laminated, and the geometry changes from basin-fill to drape. The unit is not present in the southernmost part of the survey (Fig. 7). This unit coincides with the Mass Transport Deposits (MTDs) originating from the Zanclean megaflood (see Section 3.4 Data Interpretation). The Miocene-Pliocene boundary (M-P traced with a red line in Figs. 5–7) can therefore be

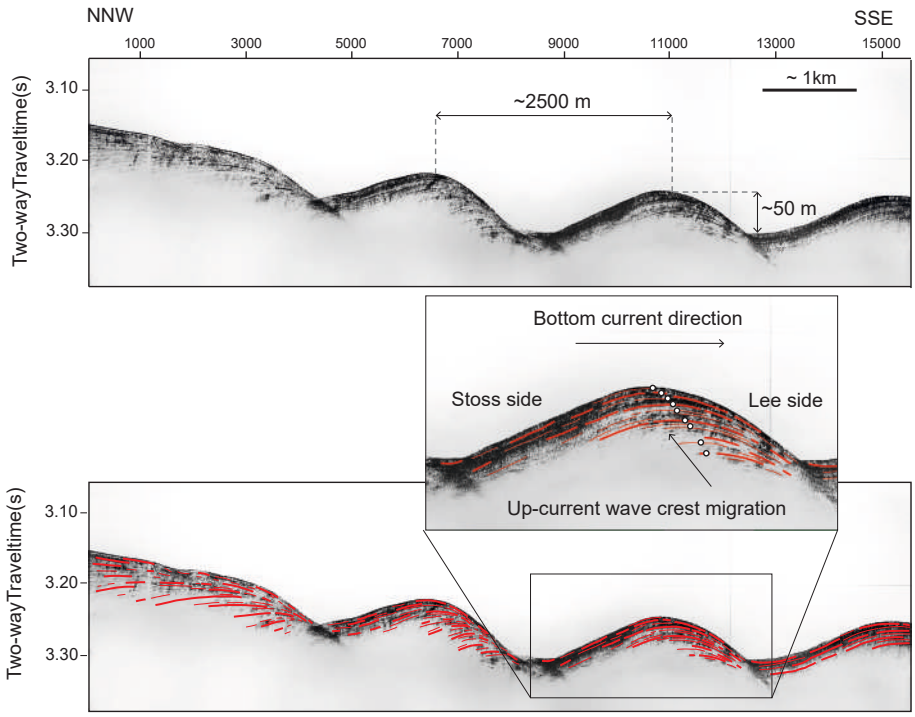

Fig. 4. CHIRP sub-bottom profile (acquired simultaneously with bathymetry) showing the internal character of the seafloor undulations. The internal reflections, conformable with the seafloor topography, show a thinning and pinching-out on the steeper SSE flank and crest migration towards the gentler NNW flank. The inferred SSE flow direction and respective stoss and lee flanks of the undulations are also shown. Location is displayed in Fig. 1.

confidently identified by following the tie to the existing seismic-stratigraphic data, and is delineated by the top of Unit 2 (Zanclean Megaflood deposit) where present, or the top of UU.

4.3.2. *Post-Messinian units*

The seismic character of Unit 1, overlying the Miocene-Pliocene boundary, is extremely variable, and is further subdivided from top-down into subunits a_1, a_2, b, c.

In the northern part of the study area (Fig. 5) the complex topography of the Zanclean flood deposit includes a large channel about 2 km wide in the middle part of Fig. 5 (profile CU15-01 approximately between SP 500 and 600, ~3.7 s TWTT), which is filled by Unit 1c markedly onlapping Unit 2 with a poor to moderate lateral continuity of reflections. There is a clear trend of increasing reflection continuity from NNW to SSE. The upper boundary of Unit 1c is erosional, as demonstrated by reflection truncations. Above is Unit 1b, an apparently transparent to chaotic seismic lens-shaped sedimentary body terminating at about SP 800 and reappearing in the form of two thin isolated lenses further to the SSE.

Unit 1b correlates with the MTD defined by Spatola et al. (2020) and is not present in the southern sector of the study area (missing in Figs. 6 and 7).

Above Unit 1b is Unit $1a_2$, which is characterized by high-amplitude reflections with a highly variable internal configuration, comprising small channel systems (width not exceeding 200–300 m) with levees, mounds outlined by reflection divergence, frequent reflection terminations denoting erosion, downlap and onlap terminations. Small lenses of apparently transparent acoustic facies are also present. From bottom to top a wavy internal configuration is gradually more distinguishable. In the northern part (Fig. 5) numerous undulations defining discontinuous sediment waves are visible. Their dimensions show significant variation, which indicates irregular growth and/or that the rate of migration was not constant, and they display frequent cross-cutting structures. Sediment wave asymmetry in Unit $1a_2$ often displays opposite trends (compare wave shapes at S.P. 200–300 with S.P. 400–500 in Fig. 5).

The character of Unit $1a_2$ is different in the southern part of the survey (Fig. 6). The variety of internal configurations seen in the northern part of the survey is not found and the unit is dominated by continuous reflections that fill the gentle topography of the distal part of the megaflood deposit (Unit 2), displaying moderate reflection divergence alternating with channel-fill and drape characters. However, one asymmetric sediment wave with a gentler, thicker NNW flank and a steeper, thinner SSE flank is visible (Fig. 6, S.P. 4500–4400). It grows above the subparallel and conformable layers of the lowermost part of Unit $1a_2$, which uniformly drape the underlying convex shape of the top of Unit 2, and then distinctly migrate through time towards the NNW. Moreover, in the upper part of Unit $1a_2$ at least two sediment waves are visible (Fig. 7, S.P. 830–430). These are asymmetric with gentler, thicker flanks towards the SSE and steeper, thinner flanks towards the NNW, indicating a migration towards the SSE of a few hundreds m.

4.3.3. *Onset of Sediment Waves unit*

A regional continuous reflection separates Unit $1a_2$ from the overlying Unit $1a_1$. We name this reflection Onset of Sediment Waves (OSW) (Figs. 5–7). This reflection marks the appearance of well-developed and steadily migrating sediment waves all along the foot of the Malta Escarpment, although evidence of sparse sediment waves is found also in the underlying Unit $1a_2$. Unit $1a_1$ is dominated by asymmetric undulations with a gently-sloping flank towards the NNW and a wavelength around 2.5 km. Wave amplitude generally increases upwards and there is a consistent migration of wave crests to the NNW of 1.0–1.5 km. Although in some cases seismic reflections seem displaced due to the thinning of the reflections along the steep SSE flank of the sediment waves (especially where erosion or non-deposition occurs), in most cases individual reflections can be traced across the troughs of the sediment waves, from one wave to the next. The steady growth and migration is more evident (persisting throughout the entire unit) in the northern part (Fig. 5), but it is clearly observable also in the southern part (Fig. 6, especially between SP 4800 and 4100, and Fig. 7). However, this pattern is more complicated in the southern part, where only a few sediment

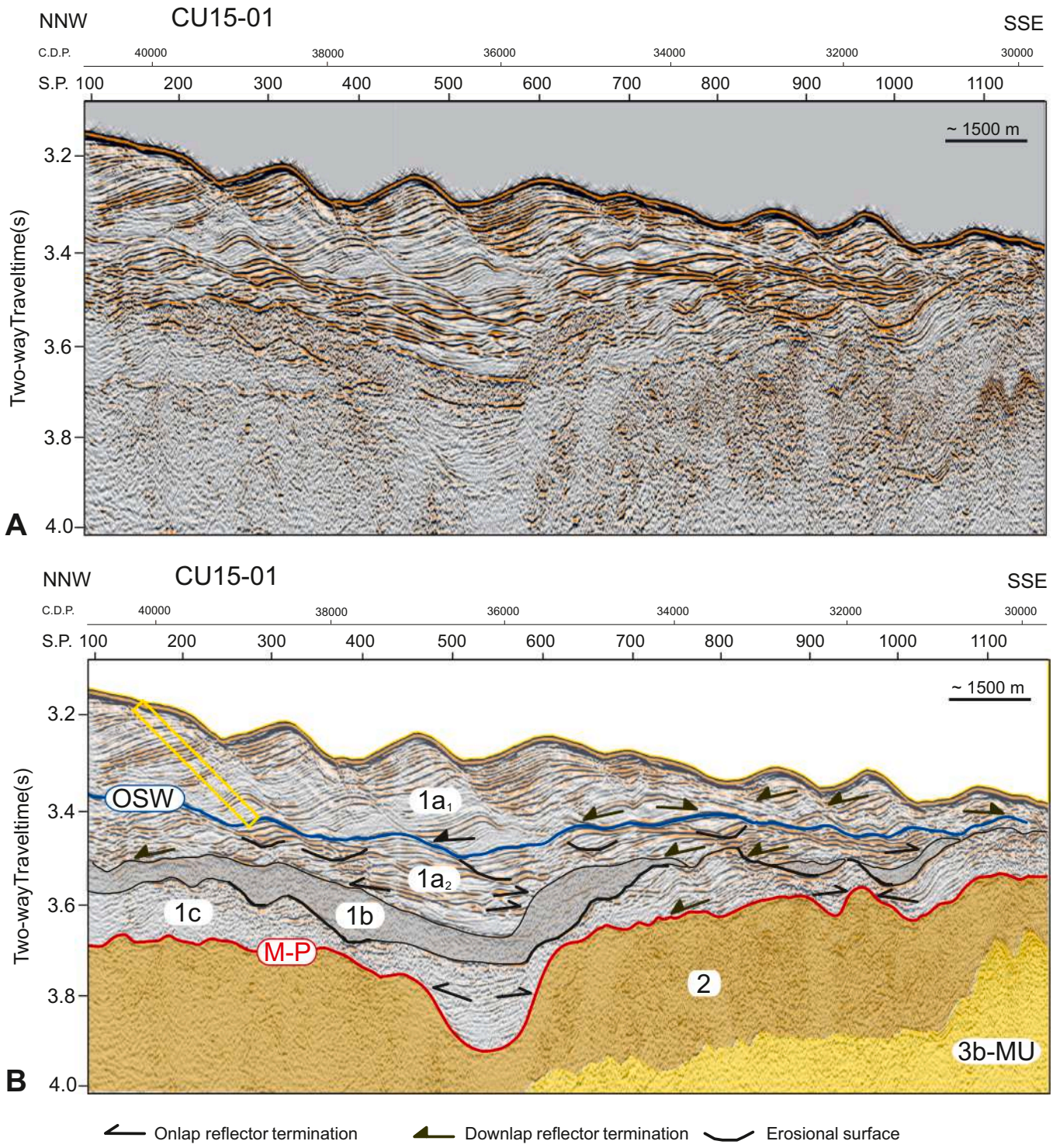

Fig. 5. Multichannel seismic reflection profile showing the internal geometry of the seafloor undulations offshore Siracusa. A) Uninterpreted profile. B) Interpreted profile following a modified stratigraphic scheme of Spatola et al. (2020). $1a_1$ = Pleistocene succession deposited after the onset of growth of sediment waves; OSW = Onset of Sediment Waves; $1a_2$ = Pleistocene succession deposited before the onset of growth of sediment waves and after the deposition of MTD 1b; 1b = Quaternary Mass Transport deposits (MTD); 1c = Early Pliocene turbidites and pelagics; M-P = Miocene- Pliocene Boundary; Unit 2 = Upper Chaotic Body Zanclean Megaflood Deposit; 3b-MU = Mobile Unit (Messinian halite). 3a-UU = Upper Unit (Messinian Gypsum) is missing in this area. Yellow rectangular areas identify sections of seismic profiles illustrated in Fig. 8. Location is displayed in Fig. 1. See text for details. (For interpretation of the references to colour in this figure legend, the reader is referred to the web version of this article.)

waves show steady growth from the bottom of the unit to the seafloor. In the uppermost part of the unit (less than 100 ms TWTT), the geometry is more complex, with some crests appearing displaced towards the NNW with respect to the lower part of the unit (e.g. Fig. 6 from about SP 4550 to 4600) or several undulations being smoothed in a single undulation (e.g. Fig. 6 between about SP 4650 to 4950). This is also apparent in Fig. 7, though the lateral continuity of the reflections in the uppermost part of the unit is more frequently interrupted by apparent diffractions

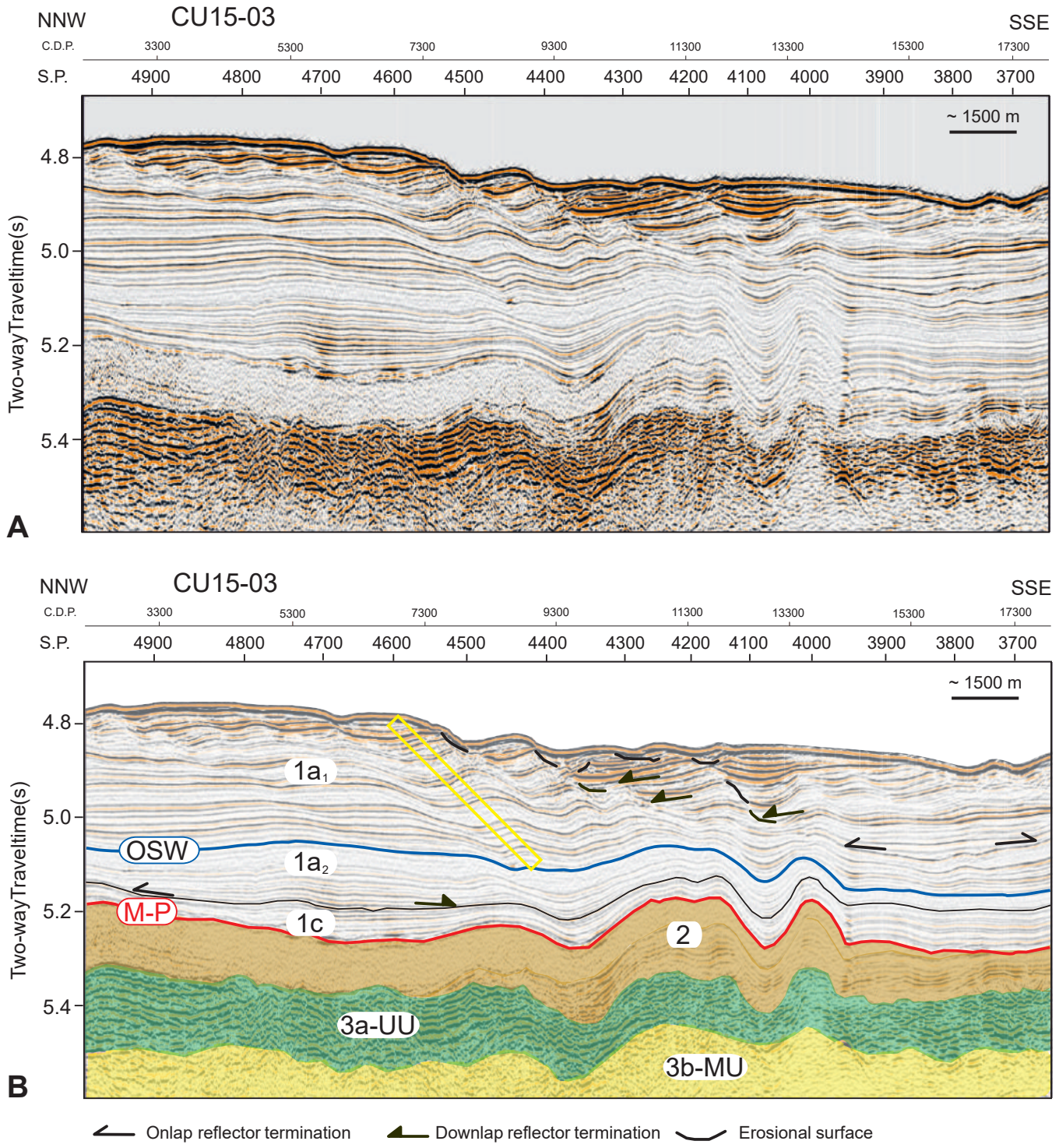

Fig. 6. Multichannel seismic reflection profile showing the internal geometry of the seafloor undulations at the foot of the Malta Escarpment west of the Malta Island. A) Uninterpreted profile. B) Interpreted profile following a modified stratigraphic scheme of Spatola et al. (2020). $1a_1$ = Pleistocene succession deposited after the onset of growth of sediment waves; OSW = Onset of Sediment Waves; $1a_2$ = Pleistocene succession deposited before the onset of growth of sediment waves; 1c = Early Pliocene turbidites and pelagics; M-P = Miocene- Pliocene Boundary; Unit 2 = Upper Chaotic Body Zanclean Megaflood Deposit; 3a- UU = Upper Unit (Messinian Gypsum); 3b-MU = Mobile Unit (Messinian halite). Yellow rectangular areas identify sections of seismic profiles illustrated in Fig. 8. Location is displayed in Fig. 1. See text for details. (For interpretation of the references to colour in this figure legend, the reader is referred to the web version of this article.)

associated with a dog-leg in the profile. In general, the thickness of the wavy unit varies between 300 and less than 100 ms TWTT. The waves are best preserved where the unit is thickest.

The seismic succession in each sediment wave is made of a regularly spaced alternation of reflectivity packages and low-reflectivity, nearly transparent, packages. Overall, reflection amplitude increases upwards. We can identify a regular succession of five sub-units between OSW and the seafloor throughout the study area (Figs. 5–7), each with high-amplitude reflections at the base that decrease upward more or less gradually in amplitude, to become nearly transparent at the top, where they are in turn overlain by the high-amplitude reflections of the sub-sequent sub-unit (Fig. 8). The thickness of the sub-units is highly

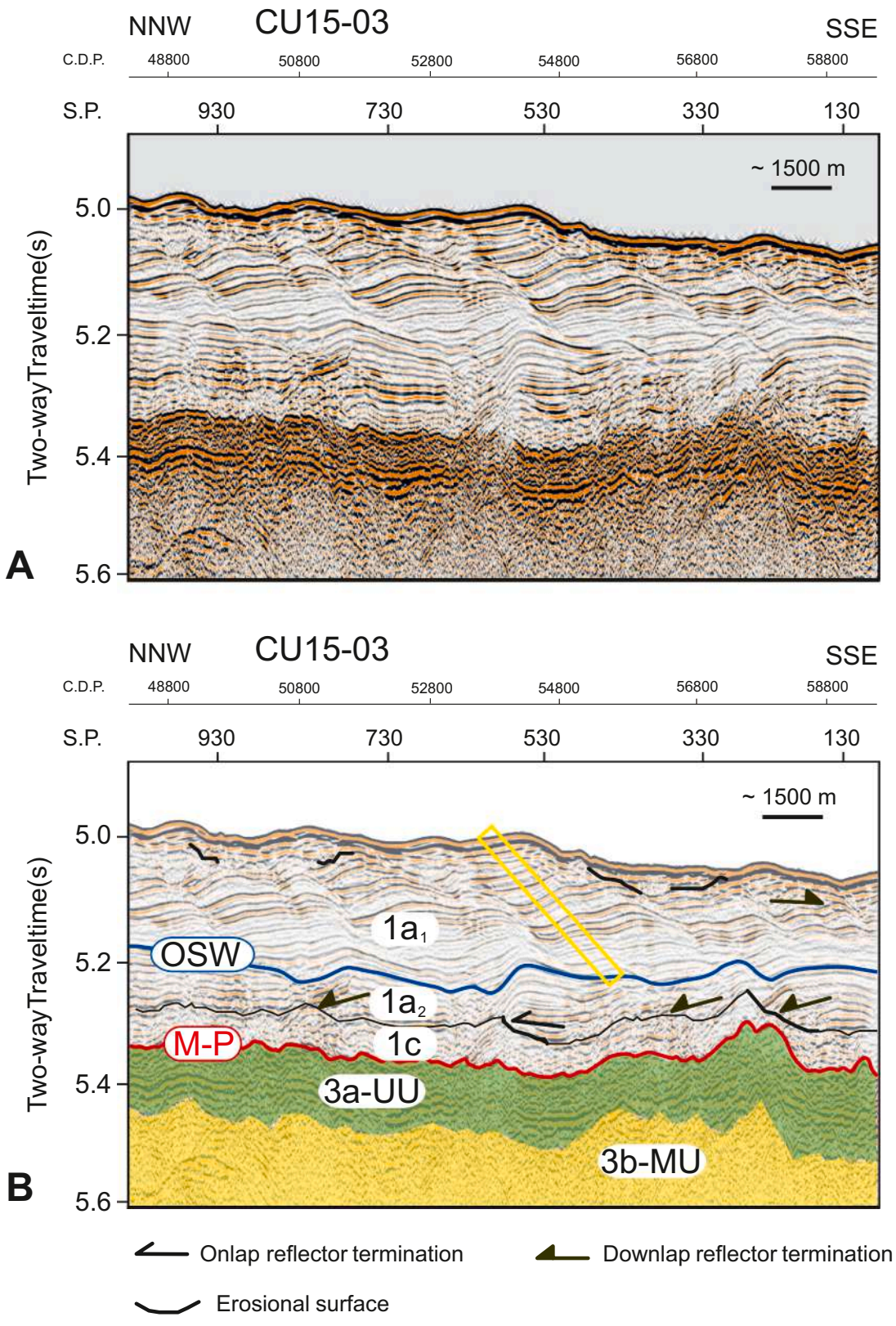

Fig. 7. Multichannel seismic reflection profile showing the internal geometry of the seafloor undulations at the foot of the southern part of the Malta Escarpment. A) Uninterpreted profile. B) Interpreted profile following a modified stratigraphic scheme of Spatola et al. (2020). $1a_1$ = Pleistocene succession deposited after the onset of growth of sediment waves; OSW = Onset of Sediment Waves; $1a_2$ = Pleistocene succession deposited before the onset of growth of sediment waves; 1c = Early Pliocene turbidites and pelagics; M-P = Miocene- Pliocene Boundary; Unit 2 = Upper Chaotic Body Zanclean Megaflood Deposit; 3a- UU = Upper Unit (Messinian Gypsum); 3b-MU = Mobile Unit (Messinian halite). Yellow rectangular areas identify sections of seismic profiles illustrated in Fig. 8. Location is displayed in Fig. 1. See text for details. (For interpretation of the references to colour in this figure legend, the reader is referred to the web version of this article.)

variable, with the thinnest being U2 in Fig. 7 (0.028 ms, ~24 m), the thickest being U5 in Fig. 7 (0.138 ms, ~116 m) and the mean thickness being 0.053 ms or ~ 44 m. The lowest sub-unit is generally the thickest, followed by sub-units of decreasing thickness with the uppermost one being again thicker. A similar trend, initially decreasing and then increasing at the top, is observable also for the thickness of the high-amplitude package of each sub-unit (highlighted in yellow in Fig. 8).

4.3.4. Litho- and chrono-stratigraphy

The area of the seafloor covered by the sediment waves considered in this study has never been sampled by coring and drilling. As a consequence there is no direct information on lithology, sedimentology or stratigraphy. DSDP Site 374, recovered a 457.5 m long succession, with limited core recovery, including a 381.2 m long Plio-Quaternary, mainly terrigenous sedimentary succession. ODP Site 964 contains a 112.2 m long, full-recovery condensed hemipelagic succession of early Pliocene to Holocene age (Fig. 9). Both sedimentary successions display an increasing terrigenous component and an increasing sedimentation rate upwards.

In Site 374, a lithologic change from nannofossil marl and mud (Unit 1B) below, to nannofossil marls with graded foraminiferal quartzose sand and silt (Unit 1A) above occurs between 100 and 110 mbsf, with a Quaternary sedimentation rate of 0.154 mm a^{-1}. The lithologic transition in Site 374 coincides with the base of turbidite layer TTL. Its age was estimated by Hieke (2000) 650 ka with an error of 100 ka, extrapolated from the constant sedimentation rate. The Quaternary sedimentation rate of 0.154 mm a^{-1} calculated for DSDP Site 374 must be corrected for the instantaneous deposition of the three megaturbidites. Assuming the thickness maps of Hieke and Werner (2000) and Hieke (2000), AT is ~10 m, DTL ~ 4 m and TTL ~ 27 m, totalling 41 m. The resulting Quaternary sedimentation rate is 0.129 mm a^{-1} and the age of TTL averaged for the 100–110 m thickness range of unit 1B is ~500 ka.

In Site 964 there are no major lithologic transitions in the Plio-Quaternary, and it is all composed of nannofossil clay, clayey nannofossil ooze, and nannofossil ooze. However, above ~25 mbsf, an increase in quartz content, clay fraction and foraminifera combined with a decrease in nannofossil content coincides with an increase in sedimentation rate from 0.023 to 0.063 mm a^{-1}. This change further reflects an upwards increase of the variability in sea surface temperature from alkenone unsaturation index (U_{37}). The age of this transition cannot be younger than 460 ka corresponding to the Lower Occurrence of *G. Lacunosa*.

Therefore, the two wells indicate that in both the abyssal plain and on surrounding abyssal hills, there is one main lithologic change that occurred during the Plio-Quaternary. This change reflects increased terrigenous sedimentary input and increasing sedimentation rate at ~460 ka.

We correlate this lithologic change to the seismic reflection OSW representing the only regional marker of a drastic change in sedimentary style reflecting the onset of sediment wave deposition, whose age can be placed between ~460 and 500 ka (Mid-Pleistocene) (Fig. 10).

Virtual seismic traces were extracted from each of the seismic profiles displayed in Figs. 5 and 6, and virtual traces were extracted from the seismic profiles displayed in Figs. 7, all representing a best estimate of the sedimentary succession above the OSW reflection (Fig. 11A, Figs. S2A, S3A). Fig. 11B,C, S2B,C and S3B,C display the resulting virtual traces and their conversion to age-domain assuming a linear age model between the OSW (500 ka) and seafloor reflections (0-age). The normalized power spectra of these virtual traces are shown in Fig. 11D, S2D and S3D.

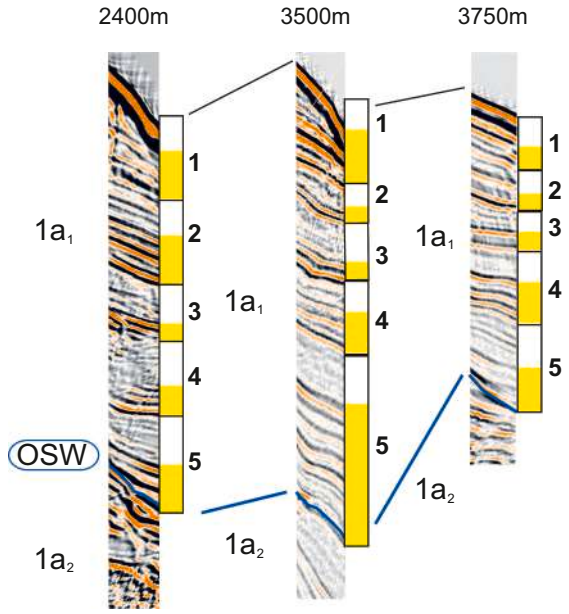

Fig. 8. Sections of seismic reflection profiles extracted perpendicularly to bedding within most representative sediment waves in Unit $1a_1$. See yellow rectangular areas in Figs. 5–7 respectively for their location. Each sediment wave appears to be composed of an alternation of 5 sub-units made of repeated pairs of high- and low-amplitude reflection packages, numbered from 1 to 5. (For interpretation of the references to colour in this figure legend, the reader is referred to the web version of this article.)

5. Discussion

5.1. Modern hydrographic conditions and actively migrating sedimentary waves

We identify a wide field of undulations in the elongated bathymetric low between the Malta Escarpment and the Calabrian Accretionary Wedge (Fig. 3).

Similar undulating seabed geometry and subseafloor strata may be generated by soft sediment deformation, for example, creep (e.g. Rebesco et al., 2009; Li et al., 2016). According to the criteria discussed in Wynn and Stow (2002), such an origin is excluded for the following reasons:

1) Creep folds do not display lateral migration and sediments on either flank of individual folds are identical.
2) Creep folds show clear evidence of displacement along fault planes and individual reflections cannot be traced across the troughs.
3) Creep folds are oriented parallel to the slope and are generally arcuate in plane view, without bifurcation.

The internal wavy geometry generally shows conformable reflections that are widely spaced on the NNW flank of the undulations, and closely spaced or even truncated on the SSE flank (Fig. 4). This geometry is common for sediment waves that actively migrate by increased sedimentation rate on the upcurrent flank and reduced sedimentation or erosion on the downcurrent flank (Wynn and Stow, 2002). Sediment waves are generated beneath currents flowing over the seabed either in the form of downslope-flowing turbidity currents (e.g. Normark and Piper, 1991; Normandeau et al., 2019), alongslope-flowing bottom currents (e.g. Flood, 1988; Baldwin et al., 2017) and internal waves (e.g. Ribó et al., 2016; Li et al., 2019).

We exclude an origin by downslope-flowing turbidity currents for the following reasons (analogous with the criteria suggested by Wynn and Stow, 2002):

1) most turbidity current waves occuring in turbidite environments, are situated on channel levees, which are not identified in the “turbidite

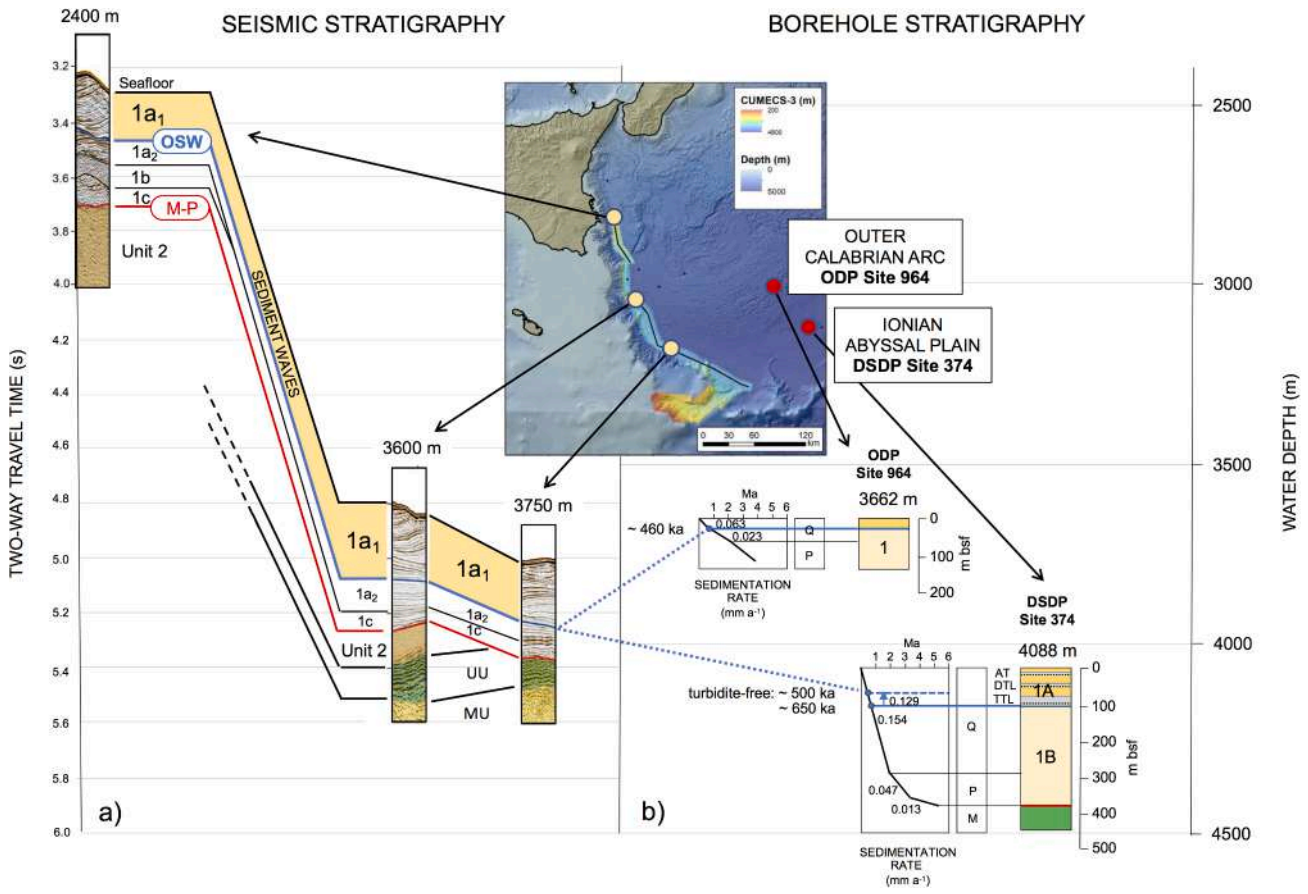

Fig. 9. Correlation of seismic units along the foot of the Malta Escarpment and to the lithostratigraphic record of DSDP SIte 274 and ODP Site 694 in the Ionian Basin. The seismic unit containing the sediment waves ($1a_1$) correlates with lithostratigraphic Unit 1A in Site 374, marked by the occurrence of megaturbidites, and to only the upper part of lithostratigraphic Unit 1 of Site 693, corresponding to an increase in sedimentation rate. Based on this seismic-borehole correlation the age of the Onset of Sediment Wave (OSW) is identified ~500 ka. For the Explanation of Seismic Units see the captions of Figs. 5–7.

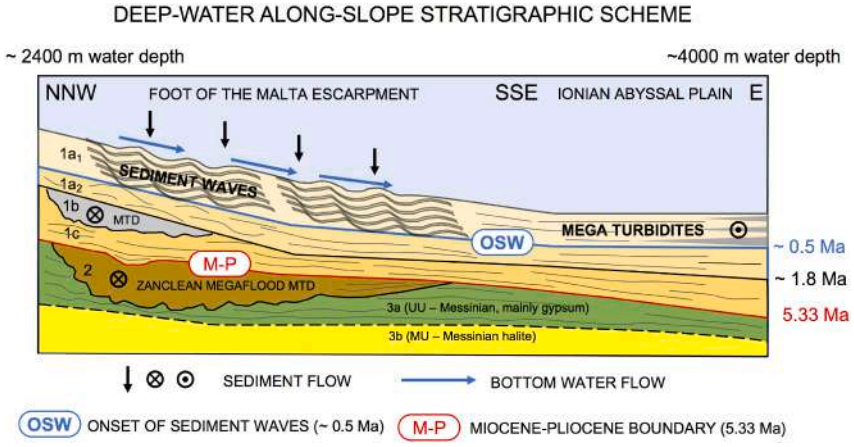

Fig. 10. Stratigraphic scheme illustrating the lateral extent of the seismic succession along the foot of the Malta Escarpment and its prolongation to the Ionian Abyssal Plain. Sediment waves at the foot of the Malta Escarpment, and megaturbidites in the abyssal plain mark the sedimentary patterns after the MPT, once the 100 ka climatic cyclicity is well established (after 500 ka - OSW and overlying Unit $1a_1$). The sediment waves record 5 glacial cycles as repetition of high- and low-amplitude reflection packages. Evidence of sediment waves exists in Unit 1a2, whose base is dated 1800 ka according to Spatola et al. (2020). A large Mass Transport Deposit (Unit 1b) is present at the foot of the NNW side of the section, with provenance from the Malta Escarpment-Sicily margin, dated 1800 ka (Spatola et al., 2020). Unit 2 represents the Zanclean megaflood deposit (Micallef et al., 2018, 2019).

valley" (Gutscher et al., 2016; San Pedro et al., 2017) at the base of the sediment-starved Malta Escarpment;

2) turbidity current waves are scarce in basin floor environments, where their crest alignment is normally slope-parallel or oblique to the regional slope if found on levee backslopes, whereas in this case the crest alignment is almost perpendicular to the Malta Escarpment;
3) turbidity current waves usually show a progressive decrease in dimension downslope, which is not observed here;
4) in turbidity current wave fields, the stratigraphic interval over which the waves occur often shows a progressive downslope thinning (up to 40–60%) associated to upslope sourcing, which is not observed here;

Though the area is affected by internal solitary waves as identified by satellite SAR images (e.g. Alpers et al., 1996), we further exclude an origin by interaction of internal waves with the continental margin, as the characteristics of the sediment waves produced by internal waves reported in the neighbouring Messina Strait area (Droghei et al., 2016)

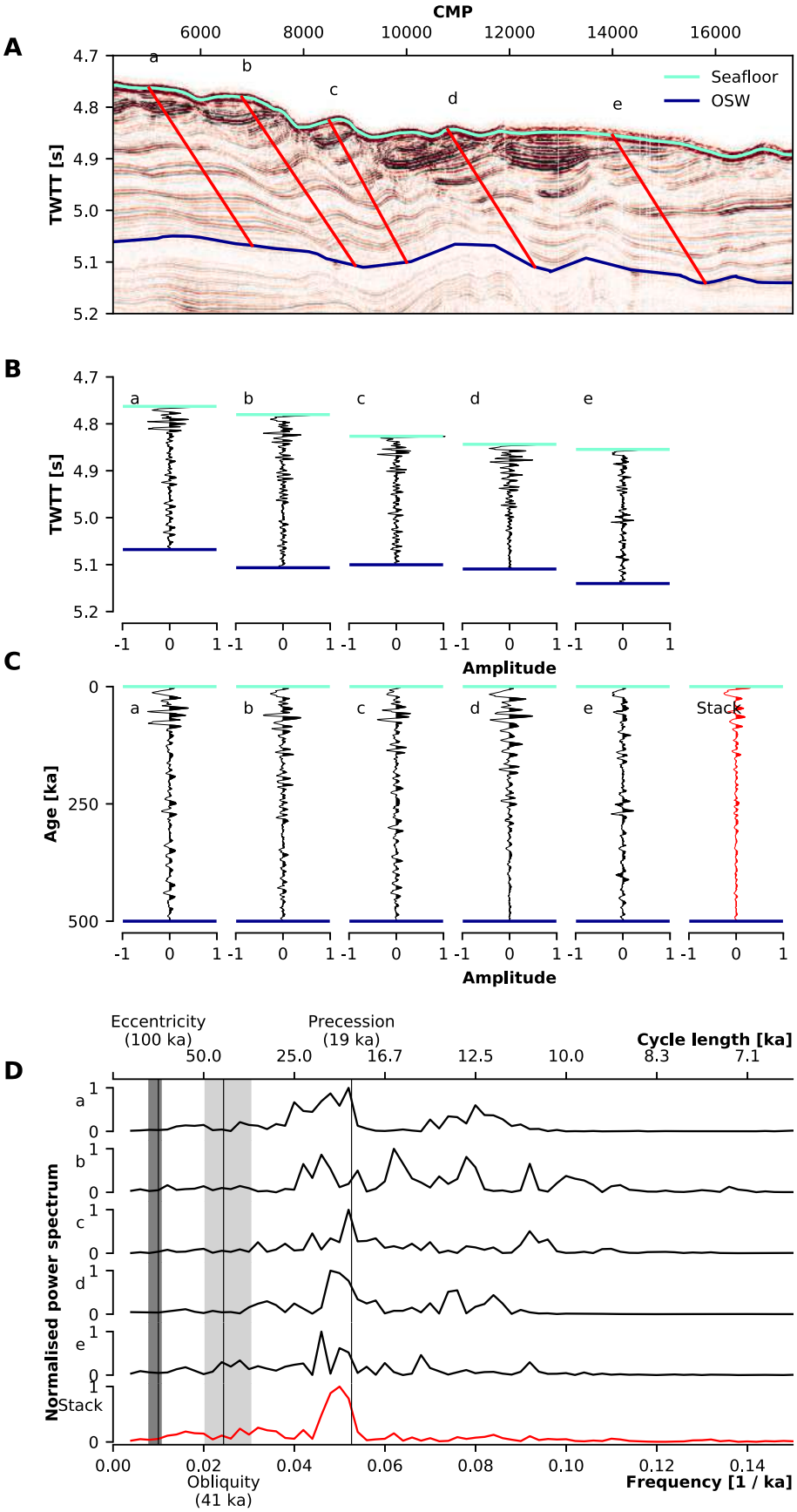

Fig. 11. Seismic cyclostratigraphic analysis (corresponding to Fig. 6). a) Section of seismic profile CU15-03 showing location of five virtual traces (a-e) picked on the stoss flank of the sediment waves approximately perpendicular to the internal bedding, between the seafloor (light blue horizon) and the OSW reflection (dark blue horizon). b) Virtual traces in TWTT. c) Virtual traces, tapered and converted to geological age, assuming linear age model between the seafloor (present) and OSW reflections (500 ka). d) Age domain power spectra of the virtual traces, Milankovitch cyclicity highlighted. The red colour indicates the stack of the traces. See text for discussion. (For interpretation of the references to colour in this figure legend, the reader is referred to the web version of this article.)

are different:

1) sediment waves produced by internal waves form at a much shallower water depth reflecting the boundary between the Levantine Intermediate Waters and the Tyrrhenian Surface Waters (200–300 m water depth);
2) the wavelength of the sediment waves in the Messina Strait area is one order of magnitude smaller with respect to the waves at the foot of Malta Escarpment;
3) the sediment texture is sandy (consistent with the small dimension of the waves);
4) inferred bottom water velocity is 50 cm s^{-1}.

Also other reported cases of sediment waves produced by internal waves show wavelength smaller than those under study: 130–200 m (Belde et al., 2015), 280–350 m (Reeder et al., 2011), 600–650 m (Karl et al., 1986), 500–1000 m (Ribó et al., 2016).

An additional criterion to classify sediment waves is the sediment type, but unfortunately we do not have samples available. Sediment waves composed of coarse grained material generally have small dimension (<300 m wavelength and < 8 m wave height), are restricted to confined settings (channels and canyons), tend to have downslope crescentic crests, can lack internal stratigraphy and are termed "small sediment waves" (Symons et al., 2016). Conversely, "large sediment waves" (sensu Symons et al., 2016) have wavelengths of up to 7200 m and wave heights of 220 m. They exhibit mixed relief compared to the overall slope and are typically located in relatively unconfined settings where they are characterized by straight to sinuous crests. Because the sediment waves at the foot of the Malta Escarpment share these characteristics we classify them as "large sediment waves". Overall the most likely origin of the sediment waves at foot of the Malta Escarpment is thus from alongslope-flowing bottom currents, confirming the interpretation by Marani et al. (1993).

Sediment waves produced by alongslope-flowing bottom current are observed to migrate upcurrent and to have their crests aligned perpendicular to oblique (45°) with respect to the dominant flow direction (Wynn and Stow, 2002; Symons et al., 2016; McCave, 2017). These waves are formed by weakly stratified bottom currents as they pass over the sediment wave topography and generate internal lee-waves (Flood, 1988). The internal lee-waves trigger higher bottom current flow velocities on the lee flanks of the sediment waves than on the stoss flanks. This process favours enhanced deposition on the upcurrent flank and upcurrent wave migration. Wave migration is predicted to occur at flow velocities above ~9 cm s^{-1}, whereas vertical aggradation is expected at lower flow velocities. Erosion or non-deposition is expected on the downcurrent wave flank with mean bottom current flow of >16 cm s^{-1} (Flood, 1988). Blumsack and Weatherly (1989) and Blumsack (1993) confirmed this model and suggested that in areas where bottom currents show frequent variations in flow direction, waves are aligned at an oblique angle to the flow and they are arranged in very small wave fields, composed of only one or two waves. According to the internal lee-wave model, the large sediment waves at the foot of the Malta Escarpment would be produced by dominantly south flowing bottom currents with flow velocities >9 cm s^{-1} and occasionally >16 cm s^{-1} in the case of erosion/non deposition on the southern flank.

The little existing data on modern abyssal water mass circulation (Adriatic Deep Water) east of the Malta Escarpment come from field activities between 2003 and 2010 (Sparnocchia et al., 2011) and show that the predominant direction is relatively constant, though current intensity is variable (Fig. 1, Table 1). The direction is southward along the Malta Escarpment (KC2 site, with mean and persistent maximum flow respectively of 5 and 15 cm s^{-1}), and northward more farther away from the escarpment (KC1, KC3 and KM3 sites with mean and maximum flow respectively of 5 and 10–12 cm s^{-1}). As mentioned in the next chapter, past velocities may have been higher, and thus the sediment waves were shaped by velocities close or above the higher edge of the possible measured/modelled spectrum. The origin of the bottom waters is ascribed to the Adriatic outflow waters, which interact strongly with waters of Aegean origin (Bensi et al., 2013), and its variability is attributed to mesoscale vortices (Rubino et al., 2012).

The average current field from the monthly means of MEDSEA Model Reanalyses at water depth of 2448.21 m between 1997 and 2018 illustrates the dominant southern flow of the current in the area where sediment waves have been identified (Fig. 12). The dominance of the southward flow is reflected in the steady growth of the large sediment waves (Figs. 4–7) and fits with the average of the monthly means (Fig. 12). However, significant variability of the direction and intensity of modern abyssal water mass circulation can be observed (Supplementary file S4). In spite of this variability, the flow direction is much more constrained in the mean direction along the Malta Escarpment (KC2 site) than on the sites away from the escarpment (KC1 site; Fig. S5). The more elongated variance ellipses in KC2 site with respect to KC1 site indicate a less variable, more oriented and energetic flow. Moreover, the fact that the major axis of the ellipses in KC2 site is aligned with the mean current vectors indicates that flow is relatively steady along the SSW direction.

Furthermore, following the discussion on the generation of abyssal sediment waves under geostrophic currents presented by McCave (2017), we have computed an estimate of the expected wavelengths of the sediment waves according to the modern hydraulic condition (Fig. 13). The expected wavelength of the sediment waves depends on the density stratification of the bottom waters, the Coriolis parameter and the mean current speed. As in Blumsack and Weatherly (1989), the condition for the wave growth is:

$$\frac{f}{k} \leq U \leq \frac{N}{k} \quad (1)$$

where:

- f is the Coriolis parameter = 8.7×10^{-5} s^{-1};

$$k = \frac{2\pi}{\lambda}$$

- λ is the sediment wavelength in km;
- N is the Brunt-Vaisala frequency in the bottom layer and is ~3×10^{-4} Hz, as calculated from the analysis of the existing CTD profiles in the study area (from OGS-NODC and SeaDataNet oceanographic data bases).
- U is the average bottom current speed of 5–15 × 10^{-2} m s^{-1}

The graphic solution for λ according to Fig. 13 provides an estimate of the wavelength in kilometers varying between 1 and 3.2, in good agreement with the observations (about 2.5 km).

In conclusion, the undulations at the foot of the Malta Escarpment are interpreted as large sediment waves generated by predominantly alongslope southward flowing bottom currents and they are compatible in orientation, migration trend and wavelength with modern hydraulic conditions.

5.2. Implications for hazards

The maximum thickness in TWTT of the sediment waves above reflection OSW is ~380 ms, corresponding to ~318 m converted using a P-wave velocity of 1673 m s^{-1}. This velocity is obtained by linear extrapolation between seafloor velocity (1500 m s^{-1}) and the base of the Plio-Quaternary unit (1760 m s^{-1}) according to data in Micallef et al. (2018). We were not able to use data from our own velocity analysis as we used a short-offset set up (seismic streamer of 300 m not allowing meaningful velocity analysis at over 2.000 m depth). The 1673 m s^{-1} is consistent with the extrapolation at depth of P-wave velocity measured

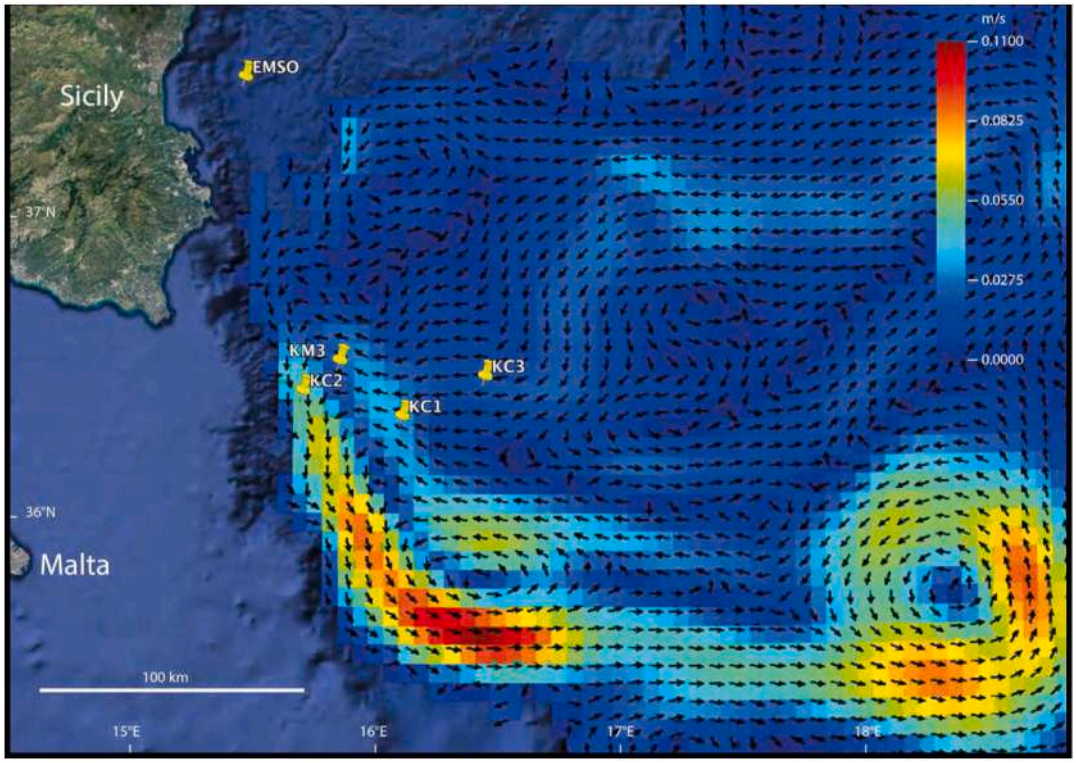

Fig. 12. Average current field (1997–2018) from the monthly means of MEDSEA model reanalyses at the level depth of 2448.21 m. The average field shows the dominant southern flow of the current at station KC2 according to the bottom topography (Simoncelli et al., 2019). Location is displayed in Fig. 1.

in ODP Site 964 split core sections with the multi-sensor core logger in the uppermost 100 m of sedimentary section (Shipboard Scientific Party, 1996). Considering the inferred age range of OSW between 460 and 500 ka, it follows that the estimated maximum sedimentary accretion at the crest of the sediment waves varies between 0.64 and 0.69 mm a^{-1}. This is a very high rate for a deep water depositional environment away from pathways of turbidity currents (0.001–0.03 · 10^{-6} mm a^{-1}(according to Lyle, 2015). It is more comparable to sedimentation rates found in coast-proximal depositional environments such as fluvial deltas and prodeltas on continental shelves (e.g. Liquete et al., 2010; 1.6–10 mm a^{-1}), or trough-mouth fans in glacial environments (e.g. Lucchi et al., 2013; 34 mm a^{-1}). Since these average rates are estimated across the glacial-interglacial cycles during the last hundreds of ka, it is most likely that during low sea level stands, where exposed continental shelves fed the deep sea with larger amounts of terrigenous sediments, net accumulation rates could have been much higher than the calculated average.

Because the overall up-current migration of the sediment wave crests has been measured between 1.0 and 1.5 km, the average annual rate of wave crest migration assuming the inferred onset varying between 460 and 500 ka is between 2.0 and 3.2 mm a^{-1}. Nevertheless, these values are obtained considering a long time interval and higher migration rates are possible. The measured velocity of bottom water currents is on average ~ 5 cm s^{-1} with peaks exceeding 10 cm s^{-1} and is compatible with sediment waves of such dimension in water depths exceeding 2500 m. Though long term variability over glacial-interglacial cycles is not known, higher velocities may have occurred.

Can these rates be considered a hazard for infrastructures deployed on the seabed? Steady vertical and horizontal sediment displacement of the order of magnitude of mm a^{-1} under a variable bottom water flow averaging 5 cm s^{-1} with peaks of 10 cm s^{-1} most probably cannot affect the stability of seabed structures with a life-time of tens of years.

Nevertheless, these values can be considered unusual for abyssal depths away from turbidity currents paths, and should be taken into due consideration in the design of deep seabed installations.

5.3. Deciphering the origin and palaeoceanographic significance of the sediment waves

5.3.1. Analysis of cyclicity as recorded by seismic data

The seismic stratigraphic analysis performed visually on the seismic sections suggests that Unit $1a_1$ overlying OSW, is composed of 5 correlatable sub-units each with high-amplitude reflections at the base and a low-amplitude package at the top (Fig. 8). OSW has been dated 460–500 ka, inferred from indirect calibration to borehole data. We can hypothesize that the 5 sub-units represent the expression of the ~100 ka orbital eccentricity Milankovitch periods in the physical properties of the sediment wave succession.

The periodicities identified in the 14 virtual seismic traces analyzed (Fig. 11, S2, S3) show some consistent correlation to Milankovitch periodicities. The longest eccentricity (100 ka) periods are very indistinct. However, obliquity (41 ka) periods match broad age-domain power spectral peaks in 9 out of the 14 virtual traces from two of the sampled sediment waves (Figs. S2D, S3D). Precession (19 ka) periods coincide fairly well with broad age-domain power spectral peaks in all the virtual traces (Figs. 11, S2D, S3D).

The weak correlation between periods extracted from virtual traces can be explained in different ways. First, there is no a priori evidence that Milakovitch cycles, or any cycles, exist in the sedimentary succession of the sediment waves. This a-priori evidence could come only from borehole data, against which seismic cyclicity in seismic data could be tested. In the present state of the knowledge, the presence of Milankovitch cycles is a hypothesis that the analysis performed fails to unambiguously demonstrate. Secondly, given the varying stratal geometry within the sediment waves, virtual traces may not be representative of the sedimentary succession exactly perpendicular to bedding. The rate of sediment accumulation within the waves is likely to be highly variable, horizontally and vertically. In particular, the glacial-interglacial deposition outlined by the 5 seismic facies patterns (sub-units) reflects varying input of terrigenous sediments into the nepheloid layer from the

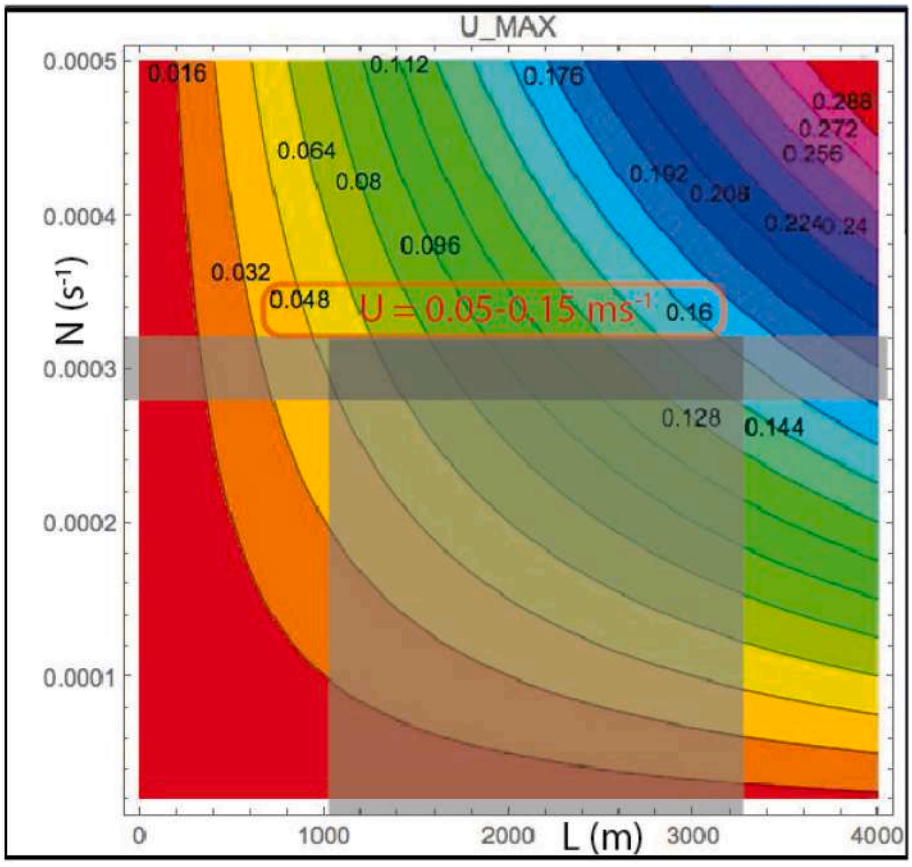

Fig. 13. Contour plot of the velocity U for the conditions for the generation of sediment waves due to bottom currents. The plot shows the maximum value of the current speed U with respect to the Brunt-Vaisala frequency N (y-axis in s^{-1}) and the wavelength of the sediment waves L (x-axis in m). For each value of U and N the wavelength of the sediment wave can be computed. In our case U = 0.05–0.15 m s^{-1} and $N = 3 \times 10\text{-}4$ Hz correspond to a wavelength between 1 and > 3 km, consistent with the field observation (wavelength of about 2.5 km).

onshore source areas, whose signal in the age domain is masked by the linear age model assumed for the conversion of the age-domain virtual traces. Furthermore, only around five major cycles are captured in the length of the virtual traces, meaning that the spectral resolution at this wavelength is relatively low. This means that peaks at, e.g., the eccentricity periodicity may not be sharp enough to be detected in these data. Tuning from thin beds with thickness below the dominant seismic wavelength can also distort the spectrum (see Mitchell, 2016).

Proper application of the method should rely on a well-constrained age model from core data, tied to individual internal seismic reflections, a seismic velocity model, and evidence of cyclicity supported by spectral analysis of proxies from core analysis, such as in Weigelt and Uenzelmann-Neben (2007) and Horn and Uenzelmann-Neben (2016). The contribution of the spectral analysis to this study is to reinforce the evidence for a highly variable rate of sediment deposition within and among each of the 5 repeated seismic facies patterns above OSW.

Cyclic deposition related to variation in bottom current velocity, rather than to variations in terrigenous input or biogenic productivity, is believed to be driven by orbital forcing (Stow et al., 1998). Beside being recognized in the sedimentary facies in outcrops on land (Stow et al., 1998) and in sedimentary cores, either from gravity corers (Lucchi and Rebesco, 2007) or from drilling (Grützner et al., 2003), such cyclicity in contourites is clearly identified in the acoustic facies of seismic reflection data, both by sparker and multichannel airgun seismic data (Stow et al., 2002b). The cyclic pattern generally observed is that of seismic facies which alternate between low reflectivity packages and relatively moderate to high amplitude reflective packages. The low reflectivity facies are attributed to a continuous succession of relatively homogeneous muddy contourites suggesting relatively low bottom current intensity, while the seismic facies containing high amplitude reflections are interpreted as the product of a succession of higher silt/sand content contourites deposited under relatively higher bottom current intensity (Stow et al., 2002b).

The best known examples of seismic facies cyclicity in contourites are from the Mediterranean and NE Atlantic area (Llave et al., 2001; Vandorpe et al., 2011; Liu et al., 2020), inferred to be influenced by changes in the circulation of the Levantine Intermediate Water (LIW) and Mediterranean Outflow Water (MOW). In the Faro-Albufeira contourite system (Gulf of Cadiz), the seismic facies cyclicity is identified in a series of Quaternary depositional sequences controlled by MOW circulation (Llave et al., 2001). An important change in the stacking pattern is inferred to occur in correspondence of the Mid Pleistocene Transition (MPT, e.g. Clark et al., 2006), from four more aggrading depositional sequences each inferred about 200 ky long, to ten clearly progradational minor sequences related to the Quaternary eccentricity cycles of 100 ky. In the Mallorca Drift, a pronounced cyclicity is recognized in the Pleistocene deposits influenced by the Balearic current that transports the LIW (Vandorpe et al., 2011). There, ten cyclical units consisting of alternating high- and low-amplitude reflection packages are identified above the MPT and correlate to MISs 1–19. In the Le Danois Drift (Bay of Biscay), four distinctive repeated units characterized by acoustically transparent, moderate amplitude and high amplitude erosional surfaces are identified between the MPT (~900–700 ka) and a late Quaternary discontinuity (~470 ka). They are compared with interglacial/glacial (100 ky) cycles that are known to have influenced the MOW and the Atlantic Mediterranean Water flow regime (Liu et al., 2020).

Seismic cycles are thus recognized in many different drifts and the regular variation of different properties through contourite successions is referred to as contourite cyclicity (Stow et al., 2019). Where this cyclicity has been drilled and dated (Gulf of Cadiz, Llave et al., 2001) it shows more or less regular 100 ka periodicity linked to Milankovitch-scale climate oscillations (Table 3). Normally, seismic cyclicity in contourites is described as a succession including a lower low-amplitude

reflection package and an upper medium-high reflectivity package, inferred to indicate a long-term increase in bottom-current velocity (Stow et al., 2019). Often, the cycles are capped by a discontinuity or hiatus in sedimentation, and then revert again to a low-amplitude reflection package (e.g. Vandorpe et al., 2011; Liu et al., 2020). Conversely, in the sediment waves at the foot of the Malta Escarpment we observe the inverse pattern: five sub-units with mean thickness of ~44 m, each consisting of lower high-amplitude packages overlain by upper low-amplitude reflection packages. The complete sediment cycle for contourites, according to the most accepted facies model linked to variation in contour-current velocity (Stow and Faugères, 2008, based on Gonthier et al., 1984), includes a coarsening-up and a fining-up cycle that defines the standard bi-gradational sequence at the scale of tens of cm to m. However, variability in the facies model has been demonstrated (Mulder et al., 2013) and the presence of either "topcut-out" and "basecut-out" partial sequences has been proposed to be equally or more common than the full bi-gradational sequence (Stow and Faugères, 2008). The alternations of seismic packages with the low-amplitude package below (e.g. Llave et al., 2001; Vandorpe et al., 2011; Liu et al., 2020) would thus resemble a "topcut-out" succession of contourite sequences, whereas the alternations of packages with the high-amplitude packages below, detected in the sediment waves at the foot of the Malta Escarpment, would thus resemble a "basecut-out" succession of contourite sequences.

5.3.2. *Onset of sediment waves: Paleoceanographic change or increased sediment input?*

The influence of bottom water circulation on sedimentation, resulting in the deposition of sediment drifts and fields of sediment waves, depends on the co-existence of sediment suspension in the water column boundary layer and appropriate bottom water flow conditions. The onset of contouritic sedimentation evolving from a non-contouritic depositional environment depends on a changing sedimentary input or a change in bottom water flow regime, or both.

Here we analyze the known paleoceanographic history of the western Ionian Basin and its sedimentary evolution to determine which factors were responsible for the onset of the sediment waves at ~500 ka when the 100 ka climatic cyclicity was well established after the MPT. We know from the geophysical survey that the sediment waves are distributed linearly along the nearly 200 km-long foot of the Malta escarpment, and from the oceanographic data analysis that they are consistent with the present-day average southward-oriented bottom water flow with peaks exceeding 10 cm s^{-1} over a muddy seafloor.

The paleo circulation of the Mediterranean Basin has been shown to reflect paleo-climate dynamics of both high- and low-latitude regions in the last 5 Ma, and the 41- to 100-ka dominant frequency shift in climate is recorded in the planktonic foraminiferal record (Colleoni et al., 2012). Water circulation changes across glacial and interglacial periods have been modelled (e.g. Myers et al., 1998; Myers, 2002) suggesting that the present-day vigorous thermohaline overturning circulation (e.g. Pinardi et al., 2019) had to be weaker during periods with wetter climatic conditions. This implies decreased evaporation and increased freshwater input from land, induced by monsoonal cycles. Deep water ventilation decreased with decreasing evaporation to the point that periods of deep water anoxia/hypoxia occurred repeatedly in the Pliocene and Pleistocene, as demonstrated by sapropel layers in deep sea sediments (e.g. Rholing et al., 2015). However, these paleoceanographic changes occurred with a periodicity reflecting the 23–19 ka precession-driven occurrence of African Monsoon climate (Negri et al., 2012). Notably, the deep sea sedimentary record of the Mediterranean Basin lacks sapropels across the MPT, reflecting a period of increased aridity in northern Africa and the eastern Mediterranean (Almogi-Labin, 2011). The onset of the sediment wave deposition at the foot of the Malta Escarpment cannot be related to periodic climatic processes of dramatic decreased overturning circulation in the Mediterranean, because these were similarly active well before and after the MPT. At a global scale, the MPT coincided with a global reorganization of the thermohaline circulation (Pena and Goldstein, 2014) with suggested enhanced deposition of contourite systems after the MPT in the NE Atlantic (Gulf of Cadiz and Cantabrian margin, Llave et al., 2001; Vandorpe et al., 2014; Liu et al., 2020) and in the Mediterranean Sea (Corsica Trough, southwestern Adriatic, and the Balearic Promontory, Amelio and Martorelli, 2008; Vandorpe et al., 2011; Miramontes et al., 2016; Pellegrini et al., 2016; Pepe et al., 2018; Barreca et al., 2018b; Gauchery et al., 2021). However, the paleo-temperature and oxygen isotopic data in the Ionian Sea (Peral et al., 2020) suggest that paleoceanographic conditions were relatively stable across the MPT.

Given the relatively stable paleoceanographic conditions across the MPT, a drastic increase in sedimentation rate at the foot of the Malta Escarpment is considered to be the main reason for consistent sediment wave generation. The inferred drastic increase of sediment input correlates to a less intense increase of sediment input into the distal Ionian abyssal plain and outer Calabrian Accretionary Wedge as demonstrated by the DSDP and ODP cores. Various evidence exists for an increased sedimentary input in the Ionian Basin in the Late Pleistocene. A major geodynamic event is identified in the Mid-Pleistocene, which is interpreted to be the result of complete slab detachment in the Calabrian subduction zone (e.g. Barreca et al., 2016), implying a drastic decrease in the rate of plate convergence from ~68 to ~2 mm a^{-1}. The consequent elastic rebound caused rapid uplift in NE Sicily (namely the Peloritan Block and the area now occupied by Mt. Etna) and in the Calabrian Block (e.g. Gvirtzman and Nur, 1999a, 1999b; Ferranti et al., 2010) causing a massive terrigenous sediment discharge towards the Western Ionian Sea.

In the last 500 ka, crustal faulting and associated fracturing triggered by the changes in subduction processes favoured the growth of the Mt. Etna composite stratovolcano along the Ionian coast of Sicily (e.g. Barreca et al., 2018a). The offshore sedimentary response of this event is a widespread erosional surface between the Lower-Middle Pleistocene Etnean clayey substratum and the overlying highly reflective seismic units on the upper continental slope (Barreca et al., 2018b). These are coeval with contourite drifts further north (Barreca et al., 2019). The continental margin has been dismantled by tectonic deformation (bulging induced by volcanic processes) and sediment gravity flows (Argnani et al., 2013). The increased sedimentation rate in the Late Pleistocene sedimentary record of the Ionian Sea (ODP Site 964 and DSDP Site 374; Fig. 9) and the unique megaturbitites identified in the Ionian Abyssal Plain (Hieke and Werner, 2000; Rebesco et al., 2000), demonstrate that augmented sediment flux is a regional trend in the Ionian Basin. A similar trend of increased sediment flux from land to sea favoured by the post-MPT higher amplitude 100 ka sea level oscillations, enhancing channel development on the Ebro continental margin, has been identified by Mauffray et al. (2017). The augmented sediment gravity flows may have travelled along the canyons and channels identified within the corridor between the north-western extremity of the Calabrian Accretionary Wedge and the Malta escarpment (Gutscher

Table 3
Examples of cyclicity in the seismic facies of contourite drifts.

	First appearance[1]	Units[2]	Main change	Sub-units[3]	Cyclicity
Llave et al., 2001	~1800 ka	4	~900 ka	10	~100 ka
Vandorpe et al., 2011	~2400 ka	6	~900 ka	10	~100 ka
Liu et al., 2020	~3,000 ka	5	~900 ka	8	~100 ka
This work	~1800 ka (Unit $1a_2$)	1	~500 ka (Unit $1a_1$)	5	~100 ka

[1] First evidence of sediment drift/sediment waves affected by bottom currents.
[2] Number of units between sediment waves first appearance and main change.
[3] Number of sub-units between main change and seafloor.

et al., 2016; San Pedro et al., 2017).

As a matter of fact, the majority of the contourite deposits tracked along Mediterranean continental margins and along the MOW path in the North Atlantic appear to have developed following the MPT: Le Danois Drift, Bay of Biscay (Liu et al., 2020), Faro-Albufeira drift, Gulf of Cadiz (Llave et al., 2001), Pen Duick drift, Gulf of Cadiz (Vandorpe et al., 2014), Balearic margin (Vandorpe et al., 2011), Pianosa slope, Tyrrhenian Sea (Miramontes et al., 2016), Tyrrhenian margin of Calabria (Amelio and Martorelli, 2008), South West Adriatic (Pellegrini et al., 2016), Gulf of Taranto, Ionian Sea (Pepe et al., 2018), NE Sicily margin, Ionian Sea (Barreca et al., 2018b), Gela Basin, Sicily Channel (Gauchery et al., 2021).

Seismic Unit $1a_2$ (between ~1800 and 500 ka) preceding the onset of sediment wave formation (Unit $1a_1$) shows evidence of sediment waves with poor lateral and vertical continuity due to erosional surfaces and lateral facies changes. We thus suggest that the bottom current regime during Unit $1a_2$ deposition was enough energetic to prevent the development of steady sediment waves with a low sedimentary input from surrounding landmasses. The following onset of sediment waves growth after ~500 ka was caused by a drastic increase in sediment input combined with the onset of a steady, overall lower energy bottom current regime installed during the last 100 ka climatic oscillations. We cannot infer in the sedimentary environment the glacial-interglacial change suggested by the clear seismic facies pattern repetition. The precession-driven episodes of decrease, or cessation, of deep water ventilation leading to sapropel depositions do not show up in the seismic record of the sediment waves. Only a weak signal for the potential of this preservation is provided by cyclicity analysis in some of the studied sediment waves. The appearance of well developed and steadily migrating sediment waves on this margin seems thus related to an increase in the sediment suspended in the water column boundary layer possibly coupled with appropriate bottom water flow conditions.

Continuous coring and physical properties logging through these continuous, expanded deep-water post MPT sedimentary successions could shed light on the climatically modulated paleo circulation changes in the Ionian Sea and increase the potential of extracting climate cycles from the seismic record.

6. Conclusions

- An elongated field of large sediment waves has been identified along the foot of the Malta Escarpment, in water depth ranging from 2400 to 3800 m.
- The sediment waves have been consistently active since ~500 ka, coinciding with the onset of the regular 100 ka climatic periodicity following the Mid-Pleistocene Transition (MPT).
- The sediment waves are consistent with the observed bottom water contouritic flow oriented south-southwestward with peaks exceeding 10 cm s^{-1}, observed in moorings.
- The crests of the sediment waves have consistently migrated upcurrent.
- The chronostratigraphic and geometric reconstruction give an estimated rate of sedimentation of between 0.64 and 0.69 mm a^{-1} and an estimated lateral migration of wave crests of between 2.0 and 3.2 mm a^{-1}. These rates are unusually high for a deep sea environment, away from downslope sediment mass transport and point to a highly dynamic deep sea bottom current-controlled sedimentary environment.
- The seismic facies of the sediment waves retain a well preserved succession of 5 visually discernible, regularly spaced sub-units consisting of an alternation of high-amplitude and low-reflectivity packages, suggesting that 100 ka orbitally-driven Milankovitch climatic oscillations are preserved.
- The not well constrained age model within the sediment wave successions prevents extracting information of climatic cyclicity from the seismic traces. Nevertheless, age-domain power spectra obtained from 14 virtual seismic traces indicate that a climatic signal of inclination and precession cycles may be preserved.
- The onset of the steady growth of sediment waves along the foot of the Malta Escarpment after ~500 ka is favoured by a dramatic increase of terrigenous sediment to the Ionian Basin as a result of tectonic uplift in NE Sicily and Calabria, which was likely accompanied by a global increased input of sediments favoured by high amplitude sea level changes after the MPT.
- Paleoceanographic changes across the MPT are not considered essential for the development of the sediment waves. Nevertheless, a possible overall decrease of bottom current intensity and relatively steady and consistent bottom water flow installed after the MPT may have contributed to the excellent preservation of the vertical and lateral continuity of the sedimentary record.
- The sediment waves along the foot of the Malta Escarpment are an excellent candidate for the extraction of a high resolution ultra-deep water sedimentary record of the paleoceanographic evolution of the Ionian Basin. This record has the potential to be relatively continuous, at least for its uppermost part (last 500 ka?), especially when obtained by composition from multiple cores.

Supplementary data to this article can be found online at https://doi.org/10.1016/j.margeo.2021.106596.

Data availability

The seismic data acquired during the CUMECS-3 survey (Camerlenghi, 2021), on which we base our observations, are available from the following doi: https://doi.org/10.6092/SNAP.afa48302-0d8e-e5e8-2962-95e136567f65

The bathymetric data were published in Gutscher et al., 2017.

The oceanographic data used in this work were published in Sparnocchia et al., 2011 and are complemented by the dataset of Lo Bue, 2019 (http://www.moist.it/sites/western_ionian_sea/2/SN12019/adcp/74/dataset/download) and Copernicus reanalysis of Simoncelli et al., 2019 (doi: 10.25423/MEDSEA_REANALYSIS_PHYS_006_004).

Declaration of Competing Interest

The authors declare that they have no known competing financial interests or personal relationships that could have appeared to influence the work reported in this paper.

Acknowledgments

Cruise CUMECS-3 of the R/V OGS Explora was funded by OGS within an agreement of scientific cooperation with the University of Malta. Captain and ship-board party are warmly thanked for the support provided during the cruise. Authors are grateful to the Italian and Maltese authorities for oceanographic survey permissions.

A.M. received funding from Marie Curie Career Integration Grant PCIG13-GA-2013-618149 within the 7th European Community Framework Programme and European Research Council (ERC) under the European Union's Horizon 2020 Research and Innovation Programme (grant agreement No 677898, MARCAN). J.F. was supported by a Marie Curie Doctoral Fellowship through the SLATE Innovative Training Network within the European Union Framework Programme for Research and Innovation Horizon 2020 under Grant Agreement No. 721403.

The study is further based upon work from COST Action "Uncovering the Mediterranean salt giant" (MEDSALT) supported by COST (European Cooperation in Science and Technology).

We thank Paradigm and IHS for providing access to ECHOS and KingdomTM (kingdom.ihs.com) software packages for the integrated interpretation of bathymetry data and Multichannel seismic reflection and sub-bottom profiles.

References

Almogi-Labin, A., 2011. The paleoclimate of the Eastern Mediterranean during the transition from early to mid Pleistocene (900 to 700 ka) based on marine and non-marine records: an integrated overview. J. Hum. Evol. 60, 428–436.

Alpers, W., Brandt, P., Rubino, A., Backhaus, J.O., 1996. Recent contributions of remote sensing to the study of internal waves in the straits of Gibraltar and Messina. In: Briand, F. (Ed.), Dynamics of Mediterranean Straits and Channels., CIESM Science Series n°2, 17. Bulletin de l'Institut océanographique, Monaco, pp. 21–40.

Amelio, M., Martorelli, E., 2008. Seismo-stratigraphic characters of paleocontourites along the Calabro-Tyrrhenian margin (Southern Tyrrhenian Sea). Mar. Geol. 252, 141–149.

Argnani, A., Mazzarini, F., Bonazzi, C., Bisson, M., Isola, I., 2013. The deformation offshore of Mount Etna as imaged by multichannel seismic reflection profiles. J. Volcanol. Geotherm. Res. 251, 50–64.

Baldwin, K.E., Mountain, G.S., Rosenthal, Y., 2017. Sediment waves in the Caroline Basin suggest evidence for Miocene shifts in bottom water flow in the western equatorial Pacific. Mar. Geol. 393, 194–202.

Barreca, G., Scarfì, L., Cannavò, F., Koulakov, I., Monaco, C., 2016. New structural and seismological evidence and interpretation of a lithospheric-scale shear zone at the southern edge of the Ionian subduction system (Central-Eastern Sicily, Italy). Tectonics 35, 1489–1505.

Barreca, G., Branca, S., Monaco, C., 2018a. Three-dimensional modeling of Mount Etna volcano: volume assessment, trend of eruption rates, and geodynamic significance. Tectonics 37, 842–857.

Barreca, G., Corradino, M., Monaco, C., Pepe, F., 2018b. Active tectonics along the South East offshore margin of Mt. Etna: new insights from high-resolution seismic profiles. Geosciences 8, 62.

Barreca, G., Scarfì, L., Gross, F., Monaco, C., De Guidia, G., 2019. Fault pattern and seismotectonic potential at the south-western edge of the Ionian Subduction system (southern Italy): new field and geophysical constraints. Tectonophysics 761, 31–45.

Bastia, R., Radhakrishna, M., Nayak, S., 2011. Identification and characterization of marine geohazards in the deep water eastern offshore of India: constraints from multibeam bathymetry, side scan sonar and 3D high-resolution seismic data. Nat. Hazards 57, 107–120.

Belde, J, Back, S, Reuning, L, 2015. Three-dimensional seismic analysis of sediment waves and related geomorphological features on a carbonate shelf exposed to large amplitude internal waves, Browse Basin region, Australia. Sedimentology 62, 87–109.

Bensi, M., Rubino, A., Cardin, V., Hainbucher, D., Mancero-Mosquera, I., 2013. Structure and variability of the abyssal water masses in the Ionian Sea in the period 2003-2010. J. Geophys. Res. Oceans 118, 931–943.

Blumsack, S., 1993. A model for the growth of mudwaves in the presence of time-varying currents. Deep-Sea Res. 40, 963–974.

Blumsack, S., Weatherly, G.L., 1989. Observations and growth mechanisms for mudwaves. Deep-Sea Res. 36, 1327–1339.

Camerlenghi, A., 2021. [Dataset] Multichannel Seismic Reflection Profiles; CUMECS3 Project. https://doi.org/10.6092/SNAP.afa48302-0d8e-e5e8-2962-95e136567f65.

Camerlenghi, A., Del Ben, A., Hübscher, C., Forlin, E., Geletti, R., Brancatelli, G., Micallef, A., Saule, M., Facchin, L., 2020. Seismic markers of the Messinian salinity crisis in the deep Ionian Basin. Basin Res. 32, 716–738.

Ceramicola, S., Rebesco, M., De Batist, M., Khlystov, O., 2002. Seismic evidence of small-scale lacustrine drifts in Lake Baikal (Russia). Mar. Geophys. Res. 22, 445–464.

Cernobori, L., Hirn, A., McBride, J.H., Nicolich, R., Petronio, L., Romanelli, M., 1996. Crustal image of the Ionian basin and its Calabrian margins. Tectonophysics 264, 175–189.

Chen, H., Zhan, W., Li, L., Wen, M.-M., 2017. Occurrence of submarine canyons, sediment waves and mass movements along the northern continental slope of the South China Sea. J. Earth Syst. Sci. 126, 73.

Clark, P.U., Archer, D., Pollard, D., Blum, J.D., Rial, J.A., Brovkin, V., Mix, A.C., Pisias, N. G., Roy, M., 2006. The middle Pleistocene transition: characteristics, mechanisms, and implications for long-term changes in atmospheric pCO2. Quat. Sci. Rev. 25, 3150–3184.

Colleoni, F., Masina, S., Negri, A., Marzocchi, A., 2012. Plio–Pleistocene high–low latitude climate interplay: a Mediterranean point of view. Earth Planet. Sci. Lett. 319-320, 35–44.

Damuth, J.E., 1979. Migrating sediment waves created by turbidity currents in the northern South China Basin. Geology 7, 520–523.

Droghei, R., Falcini, F., Casalbore, D., Martorelli, E., Mosetti, R., Sannino, G., Santoleri, R., Chiocci, F.L., 2016. The role of Internal Solitary Waves on deep-water sedimentary processes: the case of up-slope migrating sediment waves off the Messina Strait. Sci. Rep. 6, 36376.

Embley, R.W., Langseth, M.G., 1977. Sedimentation processes on the continental rise of northeastern South America. Mar. Geol. 25, 279–297.

Ferranti, L., Antonioli, F., Anzidei, M., Monaco, C., Stocchi, P., 2010. The timescale and spatial extent of vertical tectonic motions in Italy: insights from relative sealevel changes studies. J. Virtual Explor. 36, 30.

Finetti, I., 1982. Structure, stratigraphy and evolution of Central Mediterranean. Boll. Geofis. Teor. Appl. 24, 274–315.

Flood, R.D., 1988. A lee wave model for deep-sea mudwave activity. Deep-Sea Res. 35, 973–983.

Flood, R.D., Shor, A.N., 1988. Mudwaves in the argentine Basin and their relationship to regional bottom circulation patterns. Deep-Sea Res. 35, 943–971.

Fratianni, C., Clementi, E., Simoncelli, S., 2019. Quality Information Document for Med Physics Reanalysis Product: MEDSEA_REANALYSIS_PHYS_006_004. https://resources.marine.copernicus.eu/documents/QUID/CMEMS-MED-QUID-006-004.pdf.

Gačić, M., Lascaratos, A., Manca, B.B., Mantziafou, A., 2001. Adriatic Deep Water and Interaction with the Eastern Mediterranean Sea. In: Cushman-Roisin, B., Gačić, M., Poulain, P.M., Artegiani, A. (Eds.), Physical Oceanography of the Adriatic Sea. Springer, Dordrecht. https://doi.org/10.1007/978-94-015-9819-4_4.

Garcia-Castellanos, D., Micallef, A., Estrada, F., Camerlenghi, A., Ercilla, G., Periáñez, R., Abril, J.M., 2020. The Zanclean megaflood of the Mediterranean – Searching for independent evidence. Earth-Sci. Rev. 201, 103061.

Gauchery, T., Rovere, M., Pellegrini, C., Cattaneo, A., Campiani, E., Trincardi, F., 2021. Factors controlling margin instability during the Plio-Quaternary in the Gela Basin (Strait of Sicily, Mediterranean Sea). Mar. Pet. Geol. 123, 104767.

Giorgetti, A., Crise, A., Laterza, R., Perini, L., Rebesco, M., Camerlenghi, A., 2003. Water masses and bottom boundary layer dynamics above a sediment drift of the Antarctic Peninsula Pacific margin. Antarct. Sci. 15, 537–546.

Gonthier, E., Faugères, J.-C., Stow, D.A.V., 1984. Contourite facies of the Faro Drift, Gulf of Cadiz. In: Stow, D.A.V., Piper, D.J.W. (Eds.), Fine Grained Sediments, Deepwater Processes and Facies, 15. Geological Society, London, Special Publication, pp. 275–291.

Grützner, J., Rebesco, M., Cooper, A.K., Forsberg, C.F., Kryc, K.A., Wefer, G., 2003. Evidence for orbitally controlled size variations of the East Antarctic Ice Sheet during the late Miocene. Geology 31, 777–780.

Gutscher, M.A., Kopp, H., Krastel, S., Bohrmann, G., Garlan, T., Zaragosi, S., Klaucke, I., Wintersteller, P., Loubrieu, B., LeFaou, Y., SanPedro, L., Dominguez, S., Rovere, M., Mercier de Lepinay, B., Ranero, C., Sallares, V., 2017. Active tectonics of the Calabrian subduction revealed by new multi-beam bathymetric data and high-resolution seismic profiles in the Ionian Sea (Central Mediterranean). Earth Planet. Sci. Lett. 461, 61–72.

Gutscher, M.-A., Dominguez, S., De Lepinay, B.M., Pinheiro, L., Gallais, F., Babonneau, N., Cattaneo, A., Le Faou, Y., Barreca, G., Micallef, A., Rovere, M., 2016. Tectonic expression of an active slab tear from high-resolution seismic and bathymetric data offshore Sicily (Ionian Sea). Tectonics 35, 39–54.

Gvirtzman, Z., Nur, A., 1999a. Plate detachment, asthenosphere upwelling, and topography across subduction zones. Geology 27, 563–566.

Gvirtzman, Z., Nur, A., 1999b. The formation of Mount Etna as the consequence of slab rollback. Nature 401, 782–785.

Hainbucher, D., Rubino, A., Klein, B., 2006. Water mass characteristics in the deep layers of the western Ionian Basin observed during May 2003. Geophys. Res. Lett. 33, L05608.

Heezen, B.C., 1959. Dynamic processes of abyssal sedimentation: erosion, transportation and redeposition on the deep-sea floor. Geophys. J. Int. 2, 142–163.

Heezen, B.C., Hollister, C.D., Ruddiman, W.F., 1966. Shaping of the continental rise by deep geostrophic contour currents. Science 152, 502–508.

Hernández-Molina, F.J., Wåhlin, A., Bruno, M., Ercilla, G., Llave, E., Serra, N., Rosón, G., Puig, P., Rebesco, M., Van Rooij, D., Roque, D., González-Pola, C., Sánchez, F., Gómez, M., Preu, B., Schwenk, T., Hanebuth, T.J.J., Sánchez Leal, R.F., García-Lafuente, J., Brackenridge, R.E., Juan, C., Stow, D.A.V., Sánchez-González, J.M., 2016. Oceanographic processes and morphosedimentary products along the Iberian margins: a new multidisciplinary approach. Mar. Geol. 378, 127–156.

Hernández-Molina, F.J., Campbell, S., Badalini, G., Thompson, P., Walker, R., Soto, M., Conti, B., Preu, B., Thieblemont, A., Hyslop, L., Miramontes, E., Morales, E., 2018. Large bedforms on contourite terraces: sedimentary and conceptual implications. Geology 46, 27–30.

Hieke, W., 2000. Transparent layers in seismic reflection records from the central Ionian Sea (Mediterranean)—evidence for repeated catastrophic turbidite sedimentation during the Quaternary. Sediment. Geol. 135, 89–98.

Hieke, W., Werner, F., 2000. The Augias megaturbidite in the central Ionian Sea (Central Mediterranean) and its relation to the Holocene Santorini event. Sediment. Geol. 135, 205–218.

Hillenbrand, C.-D., Camerlenghi, A., Cowan, E.A., Hernández-Molina, F.J., Lucchi, R.G., Rebesco, M., Uenzelmann-Neben, G., 2008. The present and past bottom-current flow regime around the sediment drifts on the continental rise west of the Antarctic Peninsula. Mar. Geol. 255, 55–63.

Horn, M., Uenzelmann-Neben, G., 2016. The spatial extent of the Deep Western Boundary current into the Bounty Trough: new evidence from parasound sub-bottom profiling. Mar. Geophys. Res. 37, 145–158.

Jungclaus, J.H., Backhaus, J.O., 1994. Application of a transient reduced-gravity plume model to the Denmark Strait overflow. J. Geophys. Res. 99, 12,375–12,396.

Karl A, H, Cacchione A, D, Carlson R, P, 1986. Internal-wave currents as a mechanism to account for large sand waves in Navarinsky canyon head, Bering Sea. J. Sediment. Petrol 56, 706–714.

Kenyon, N.H., 1986. Evidence from bedforms for a strong poleward current along the upper continental slope of NW Europe. Mar. Geol. 72, 187–198.

Li, J., Li, W., Alves, T.M., Rebesco, M., Zhan, W., Sun, J., Mitchell, N.C., Wu, S., 2019. Different origins of seafloor undulations in a submarine canyon system, northern South China Sea, based on their seismic character and relative location. Mar. Geol. 413, 99–111.

Li, W., Alves, T.M., Wu, S., Rebesco, M., Zhao, F., Mi, L., Ma, B., 2016. A giant, submarine creep zone as a precursor of large-scale slope instability offshore the Dongsha Islands (South China Sea). Earth Planet. Sci. Lett. 451, 272–284.

Li, W., Alves, T.M., Rebesco, M., Sun, J., Li, J., Li, S., Wu, S., 2020. The Baiyun Slide complex, South China Sea: a modern example of slope instability controlling submarine-channel incision on continental slopes. Mar. Pet. Geol. 114, 104231.

Liquete, C., Lucchi, R.G., Garcia-orellana, J., Canals, M., Masqué, S.P., Pasqual, C., Lavoie, C., 2010. Modern sedimentation patterns and human impacts on the Barcelona continental shelf (NE Spain). Geol. Acta 8, 169–187.

Liu, S., Hernández-Molina, F.J., Ercilla, G., Van Rooij, D., 2020. Sedimentary evolution of the Le Danois contourite drift systems (southern Bay of Biscay, NE Atlantic): a

reconstruction of the Atlantic Mediterranean Water circulation since the Pliocene. Mar. Geol. 427, 106217.
Llave, E., Hernández-Molina, F.J., Somoza, L., Díaz-del-Río, V., Stow, D.A.V., Maestro, A., Alveirinho Dias, J.M., 2001. Seismic stacking pattern of the Faro-Albufeira contourite system (Gulf of Cadiz): a Quaternary record of paleoceanographic and tectonic influences. Mar. Geophys. Res. 22, 487–508.
Lo Bue, N., 2019. [Dataset] ADCP Dataset (RDI WorkHorse 600 KHz @ 2 profile/hour) from INGV/NEMO-SN1 Seafloor Platform during EMSO-MIUR Project in Western Ionian Sea site (East Sicily), Part of EMSO Network. http://www.moist.it/sites/western_ionian_sea/2/SN12019/adcp/74/dataset/download.
Lofi, J., Sage, F., Deverchere, J., Loncke, L., Maillard, A., Gaullier, V., Thinon, I., Gillet, H., Guennoc, P., Gorini, C., 2011. Refining our knowledge of the Messinian salinity crisis records in the offshore domain through multi-site seismic analysis. Bull. Soc. Géol. Fr. 182, 163–180.
Lucchi, R.G., Rebesco, M., 2007. Glacial contourites on the Antarctic Peninsula margin: insight for palaeoenvironmental and palaeoclimatic conditions. Geol. Soc. Lond. Spec. Publ. 276, 111–127.
Lucchi, R.G., Camerlenghi, A., Rebesco, M., Urgeles, R., Sagnotti, L., Macrì, P., Colmenero-Hidalgo, E., Sierro, F.J., Melis, R., Barcena, M.A., Giorgetti, G., Villa, G., Persico, D., Flores, J.A., Pedrosa, M.T., Caburlotto, A., 2013. Postglacial sedimentary processes on the Storfjorden and Kveithola TMFs: impact of extreme glacimarine sedimentation. Glob. Planet. Chang. 111, 309–326.
Lyle, M., 2015. Deep-sea sediments. In: Harff, J., Meschede, M., Petersen, S., Thiede, J. (Eds.), Encyclopedia of Marine Geosciences. Springer, Dordrecht.
Manca, B.B., Ursella, L., Scarazzato, P., 2002. New development of eastern mediterranean circulation based on hydrological observations and current measurements. Mar. Ecol. 23, 237–257.
Manca, B.B., Budillon, G., Scarazzato, P., Ursella, L., 2003. Evolution of dynamics in the eastern Mediterranean affecting water mass structures and properties in the Ionian and Adriatic Seas. J. Geophys. Res. Oceans 108. PBE 3-1 - 3-19.
Marani, M., Argnani, A., Roveri, M., Trincardi, F., 1993. Sediment drifts and erosional surfaces in the Central Mediterranean: seismic evidence of bottom-current activity. Sediment. Geol. 82, 207–220.
Margiotta, A., 2016. Perspectives of the KM3NeT project. Nucl. Part. Phys. Proc. 279-281, 182–189.
Martin, F.D., Batalla, L.F., De Oliveira Pinheiro, R.L., Escalona, L.G., El Mistikawi, S., Tiffany, J., Pryne, D.E., Haneberg, W.C., Campbell, K.J., 2015. The integration of 3D seismic with the ultrahigh resolution data from the marine survey: Recognizing and quantifying several challenging features for subsea production installations in complex environment offshore Brazil. Proc. Ann. Offshore Technol. Conf. 5, 3260–3270.
Mauffray, M.-A., Urgeles, R., Berne, S., Canning, J., 2017. Development of submarine canyons after the Mid-Pleistocene transition on the Ebro margin, NW Mediterranean: the role of fluvial connections. Quat. Sci. Rev. 158, 77–93.
McCave, I.N., 2017. Formation of sediment waves by turbidity currents and geostrophic flows: a discussion. Mar. Geol. 390, 89–93.
McCave, I.N., Carter, L., 1997. Recent sedimentation beneath the Deep Western Boundary current off northern New Zealand. Deep-Sea Res. 7, 1203–1237.
Meccia, V.L., Borghini, M., Sparnocchia, S., 2015. Abyssal circulation and hydrographic conditions in the Western Ionian Sea during Spring-Summer 2007 and Autumn-Winter 2007-2008. Deep Sea Res. Part I Oceanogr. Res. Pap. 104, 26–40.
Micallef, A., Georgiopoulou, A., Mountjoy, J., Huvenne, V.A.I., Iacono, C.L., Le Bas, T., Del Carlo, P., Otero, D.C., 2016. Outer shelf seafloor geomorphology along a carbonate escarpment: the eastern Malta Plateau. Mediterranean Sea. Cont. Shelf Res. 131, 12–27.
Micallef, A., Camerlenghi, A., Garcia-Castellanos, D., Cunarro Otero, D., Gutscher, M.-A., Barreca, G., Spatola, D., Facchin, L., Geletti, R., Krastel, S., Gross, F., Urlaub, M., 2018. Evidence of the Zanclean megaflood in the eastern Mediterranean Basin. Sci. Rep. 8, 1078.
Micallef, A., Camerlenghi, A., Georgiopoulou, A., Garcia-Castellanos, D., Gutscher, M.-A., Lo Iacono, C., Huvenne, V.A.I., Mountjoy, J.J., Paull, C.K., Le Bas, T., Spatola, D., Facchin, L., Accettella, D., 2019. Geomorphic evolution of the Malta Escarpment and implications for the Messinian evaporative drawdown in the eastern Mediterranean Sea. Geomorphology 327, 264–283.
Miramontes, E., Cattaneo, A., Jouet, G., Théreau, E., Thomas, Y., Rovere, M., Cauquil, E., Trincardi, F., 2016. The Pianosa contourite depositional system (Northern Tyrrhenian Sea): drift morphology and Plio-Quaternary stratigraphic evolution. Mar. Geol. 378, 20–42.
Miramontes, E., Penven, P., Fierens, R., Droz, L., Toucanne, S., Jorry, S.J., Jouet, G., Pastor, L., Silva Jacinto, R., Gaillot, A., Giraudeau, J., Raisson, F., 2019. The influence of bottom currents on the Zambezi Valley morphology (Mozambique Channel, SW Indian Ocean): in situ current observations and hydrodynamic modelling. Mar. Geol. 410, 42–55.
Mitchell, N.C., 2016. Comment on: “the spatial extent of the Deep Western Boundary current into the Bounty Trough: new evidence from parasound sub-bottom profiling” by Horn and Uenzelmann-Neben. Mar. Geophys. Res. 37, 371–374.
Mosher, D.C., Campbell, D.C., Gardner, J.V., Piper, D.J.W., Chaytor, J.D., Rebesco, M., 2017. The role of deep-water sedimentary processes in shaping a continental margin: the Northwest Atlantic. Mar. Geol. 393, 245–259.
Mulder, T., Hassan, R., Ducassou, E., Zaragosi, S., Gonthier, E., Hanquiez, V., Marchès, E., Toucanne, S., 2013. Contourites in the Gulf of Cadiz: a cautionary note on potentially ambiguous indicators of bottom current velocity. Geo-Mar. Lett. 33, 357–367.
Myers, P.G., 2002. Flux-Forced Simulations of the Paleocirculation of the Mediterranean Paleoceanogrpahy 17,1009.
Myers, P.G., Haines, K., Rohling, E.J., 1998. Modeling the palcocirculation of the Mediterranean: the last glacial maximum and the Holocene with emphasis on the formation of sapropel S1. Paleoceanogrpahy 13, 586–606.
Negri, A., Colleoni, F., Masina, S., 2012. Mediterranean Sapropels: a mere geological problem or a resource for the study of a changing planet? Alp. Mediterr. Quat. 25, 81–89.
Nicolich, R., Laigle, M., Hirn, A., Cernobori, L., Gallart, J., 2000. Crustal structure of the ionian margin of Sicily: Etna volcano in the frame of regional evolution. Tectonophysics 329, 121–139.
Normandeau, A., Campbell, D.C., Cartigny, M.J.B., 2019. The influence of turbidity currents and contour currents on the distribution of deep-water sediment waves offshore eastern Canada. Sedimentology 66, 1746–1767.
Normark, W.R., Piper, D.J.W., 1991. Initiation processes and fow evolution of turbidity currents : implications for the depositional record. SEPM Spec. Publ. 46, 207–229.
Pellegrini, C., Maselli, V., Trincardi, F., 2016. Pliocene–Quaternary contourite depositional system along the south-western Adriatic margin: changes in sedimentary stacking pattern and associated bottom currents. Geo-Mar. Lett. 36, 67–79.
Pena, D.L., Goldstein, S.L., 2014. Thermohaline circulation crisis and impacts during the mid-Pleistocene transition. Science 345 (6194), 318–322. https://doi.org/10.1126/science.1249770, 1249770.
Pepe, F., Di Donato, V., Insinga, D., Molisso, F., Faraci, C., Sacchi, M., Dera, R., Ferranti, L., Passaro, S., 2018. Seismic stratigraphy of upper Quaternary shallow-water contourite drifts in the Gulf of Taranto (Ionian Sea, southern Italy). Mar. Geol. 397, 79–92.
Peral, M., Blamart, D., Bassinot, F., Daëron, M., Dewilde, F., Rebaubier, H., Nomade, S., Girone, A., Marino, M., Maiorano, P., Ciaranfi, N., 2020. Changes in temperature and oxygen isotopic composition of Mediterranean water during the Mid-Pleistocene transition in the Montalbano Jonico section (southern Italy) using the clumped-isotope thermometer. Palaeogeogr. Palaeoclimatol. Palaeoecol. 544, 109603.
Pinardi, N., Zavatarelli, M., Adani, M., Coppini, G., Fratianni, C., Oddo, P., Tonani, M., Lyubartsev, V., Dobricic, S., Bonaduce, S., 2015. Mediterranean Sea large-scale, low-frequency ocean variability and water mass formation rates from 1987 to 2007: a retrospective analysis. Prog. Oceanogr. 132, 318–332.
Pinardi, N., Cessi, P., Borile, F., Wolfe, C.P.L., 2019. The Mediterranean Sea Overturning Circulation. J. Phys. Oceanogr. 49, 1699–1271.
Polonia, A., Bonatti, E., Camerlenghi, A., Lucchi, R.G., Panieri, G., Gasperini, L., 2013. Mediterranean megaturbidite triggered by the AD 365 Crete earthquake and tsunami. Sci. Rep. 3, 1285.
Polonia, A., Torelli, L., Artoni, A., Carlini, M., Faccenna, C., Ferranti, L., Gasperini, L., Govers, R., Klaeschen, D., Monaco, C., Neri, G., Nijholt, N., Orecchio, B., Wortel, R., 2016. The Ionian and Alfeo-Etna fault zones: New segments of an evolving plate boundary in the Central Mediterranean Sea? Tectonophysics 675, 69–90.
Putans, V.A., Merklin, L.R., Levchenko, O.V., 2010. Sediment waves and other forms as evidence of geohazards in Caspian Sea. Int. J. Offshore Polar 20, 241–246.
Rebesco, M., Della Vedova, B., Cernobori, L., Aloisi, G., 2000. Acoustic facies of Holocene megaturbidites in the Eastern Mediterranean. Sediment. Geol. 135, 65–74.
Rebesco, M., Neagu, R.C., Cuppari, A., Muto, F., Accettella, D., Dominici, R., Cova, A., Romano, C., Caburlotto, A., 2009. Morphobathymetric analysis and evidence of submarine mass movements in the western Gulf of Taranto (Calabria margin, Ionian Sea). Int. J. Earth Sci. 98, 791–805.
Rebesco, M., Hernández, Molina J., van Rooij, D., Wåhlin, A., 2014. Contourites and associated sediments controlled by deep-water circulation processes: state-of-the-art and future considerations. Mar. Geol. 352, 111–154.
Reeder B, D, Ma B, B, Yang J, Y, 2011. Very large subaqueous sand dunes on the upper continental slope in the South China Sea generated by episodic, shoaling deep-water internal solitary waves. Mar. Geol. 279, 12–18. https://doi.org/10.1016/j.margeo.2010.10.009.
Rholing, E.J., Marinao, J., Grant, K.M., 2015. Mediterranean climate and oceanography, and the periodic development of anoxic events (sapropels). Earth-Sci. Rev. 143, 62–97.
Ribó, M., Puig, P., Muñoz, A., Lo Iacono, C., Masqué, P., Palanques, A., Acosta, J., Guillén, J., Gómez Ballesteros, M., 2016. Morphobathymetric analysis of the large fine grained sediment waves over the Gulf of Valencia continental slope (NW Mediterranean). Geomorphology 253, 22–37.
Robinson, A.R., Sellschopp, J., Warn-Varnas, A., Leslie, W.G., Lozano, C.J., Haley Jr., P. J., Anderson, L.A., Lermusiaux, P.F.J., 1999. The Atlantic ionian stream. J. Mar. Syst. 20 (1–4), 129–156. http://www.sciencedirect.com/science/article/pii/S0924796398000797.
Rossi, S., Sartori, R., 1981. A seismic reflection study of the External Calabrian Arc in the northern Ionian Sea (eastern Mediterranean). Mar. Geophys. Res. 4, 403–426.
Rubino, A., Falcini, F., Zanchettin, D., Bouche, V., Salusti, E., Bensi, M., Riccobene, G., De Bonis, G., Masullo, R., Simeone, F., Piattelli, P., Sapienza, P., Russo, S., Platania, G., Sedita, M., Reina, P., Avolio, R., Randazzo, N., Hainbucher, D., Capone, A., 2012. Abyssal undular vortices in the Eastern Mediterranean basin. Nat. Commun. 3, 834.
San Pedro, L., Babonneau, N., Gutscher, M.-A., Cattaneo, A., 2017. Origin and chronology of the Augias deposit in the Ionian Sea (Central Mediterranean Sea), based on new regional sedimentological data. Mar. Geol. 384, 199–213.
Schroeder, K., Borghini, M. (Eds.), 2008. SESAME-KM3 Cruise Report. CNR ISMAR – Istituto di Scienze Marine, 11–25 March 2008, p. 37.
Shipboard Scientific Party, 1978. Site 374: Messina Abyssal Plain. In: Hsü, K.J., Montadert, L., et al. (Eds.), Initial Reports of the Deep Sea Drilling Project, Volume 42, Part 1. U.S. Government Printing Office, Washington, pp. 175–218.
Shipboard Scientific Party, 1996. Site 964. In: Emeis, K.-C., Robertson, A.H.F., Richter, C., et al. (Eds.), Proceedings of the Ocean Drilling Program, Initial Reports, 160, pp. 85–123.

Simoncelli, S., Fratianni, C., Pinardi, N., Grandi, A., Drudi, M., Oddo, P., Dobricic, S., 2019. [Dataset] Mediterranean Sea Physical Reanalysis (CMEMS MED-Physics). Copernicus Monitoring Environment Marine Service (CMEMS). https://doi.org/10.25423/MEDSEA_REANALYSIS_PHYS_006_004.

Skliris, N., 2014. Past, present and future patterns of the Thermohaline Circulation and characteristic water masses of the Mediterranean Sea. In: Goffredo, S., Dubinsky, Z. (Eds.), The Mediterranean Sea: Its History and Present Challenges. DE. Springer, Berlin, pp. 29–48. https://doi.org/10.1007/978-94-007-6704-1_3.

Sparnocchia, S., Gasparini, G.P., Schroeder, K., Borghini, M., 2011. Oceanographic conditions in the NEMO region during the KM3NeT project (April 2006–May 2009). Nucl. Instrum. Methods Phys. Res. A 626-627, S87–S90.

Spatola, D., del Moral-Erencia, J.D., Micallef, A., Camerlenghi, A., Garcia-Castellanos, D., Gupta, S., Bohorquez, P., Gutscher, M.A., Bertoni, C., 2020. A single-stage megaflood at the termination of the Messinian salinity crisis: Geophysical and modelling evidence from the eastern Mediterranean Basin. Mar. Geol. 430, 106337.

Stow, D., Smillie, Z., Pan, J., Esentia, I., 2019. Deep-sea contourites: Sediments and cycles. Encyclop. Ocean Sci. 111–120.

Stow, D.A.V., Faugères, J.-C., 2008. Contourite facies and the facies model. In: Rebesco, M., Camerlenghi, A. (Eds.), Contourites, 60. Elsevier, Amsterdam, Developments in Sedimentology, pp. 223–256.

Stow, D.A.V., Faugères, J.-C., Viana, A., Gonthier, E., 1998. Fossil contourites: a critical review. Sediment. Geol. 115, 3–31.

Stow, D.A.V., Pudsey, C.J., Howe, J.A., Faugères, J.-C., Viana, A.R., 2002a. Deep-water contourite systems: modern drifts and ancient series, seismic and sedimentary characteristics. Geol. Soc. Lond. Mem. 22, 464.

Stow, D.A.V., Faugères, J., Gonthier, E., Cremer, M., Llave, E., Hernández-Molina, F.J., Somoza, L., Díaz-Del-Río, V., 2002b. Faro-Albufeira drift complex, northern Gulf of Cadiz. Geol. Soc. Lond. Mem. 22, 137–154.

Symons, W.O., Sumner, E.J., Tailing, P.J., Cartigny, M.J.S., Clare, M.A., 2016. Large-scale sediment waves and scours on the modern seafloor and their implications for the prevalence of supercritical flows. Mar. Geol. 371, 130–148.

Tallobre, C., Loncke, L., Bassetti, M.-A., Giresse, P., Bayon, G., Buscail, R., de Madron, X. D., Bourrin, F., Vanhaesebroucke, M., Sotin, C., the IGUANES Scientific Party, 2016. Description of a contourite depositional system on the Demerara Plateau: results from geophysical data and sediment cores. Mar. Geol. 378, 56–73.

Van Daele, M., Bertrand, S., Meyer, I., Moernaut, J., Vandoorne, W., Siani, G., Tanghe, N., Ghazoui, Z., Pino, M., Urrutia, R., De Batist, M., 2016. Late Quaternary evolution of Lago Castor (Chile, 45.6°S): timing of the deglaciation in northern Patagonia and evolution of the southern westerlies during the last 17 kyr. Quat. Sci. Rev. 133, 130–146.

Vandorpe, T., Van Rooij, D., de Haas, H., 2014. Stratigraphy and paleoceanography of a topography-controlled contourite drift in the Pen Duick area, southern Gulf of Cádiz. Mar. Geol. 349, 136–151.

Vandorpe, T.P., Van Rooij, D., Stow, D.A.V., Henriet, J.-P., 2011. Pliocene to recent shallow water contourite deposits on the shelf and shelf edge off south-western Mallorca, Spain. Geo-Mar. Lett. 31, 391–403.

Villa, G., Persico, D., Bonci, M.C., Lucchi, R.G., Morigi, C., Rebesco, M., 2003. Biostratigraphic characterization and Quaternary microfossil palaeoecology in sediment drifts west of the Antarctic Peninsula - Implications for cyclic glacial-interglacial deposition. Palaeogeogr. Palaeoclimatol. Palaeoecol. 198, 237–263.

Volpi, V., Del Ben, A., Civile, D., Zgur, F., 2017. Neogene tectono-sedimentary interaction between the Calabrian Accretionary Wedge and the Apulian Foreland in the northern Ionian Sea. Mar. Pet. Geol. 83, 246–260.

Weigelt, E., Uenzelmann-Neben, G., 2007. Orbital forced cyclicity of reflector strength in the seismic records of the Cape Basin. Geophys. Res. Lett. 34, L01702.

Wüst, G., 1961. On the vertical circulation of the Mediterranean Sea. Geophys. Res. 66, 3261–3271.

Wynn, R.B., Stow, D.A.V., 2002. Classification and characterisation of deep-water sediment waves. Mar. Geol. 192, 7–22.

Zenk, W., 2008. Abyssal and contour currents. In: Rebesco, M., Camerlenghi, A. (Eds.), Contourites, 60. Elsevier, Amsterdam, Developments in Sedimentology, pp. 37–57.

Zhang, W., Hanebuth, T.J.J., Stöber, U., 2016. Short-term sediment dynamics on a meso-scale contourite drift (off NW Iberia): Impacts of multi-scale oceanographic processes deduced from the analysis of mooring data and numerical modelling. Mar. Geol. 378, 81–100.

Zhao, Y., Liu, Z., Zhang, Y., Li, J., Wang, M., Wang, W., Xu, J., 2015. In situ observation of contour currents in the northern South China Sea: applications for deepwater sediment transport. Earth Planet. Sci. Lett. 430, 477–485.